Supporting Information

Arresting Dissolution of Two-Dimensional Metal-Organic Frameworks Enables Long Life in Electrochemical Devices

Gopi M. R. Dontireddy[a], Satya Prakash Suman[a], Jose L. Merino-Gardea[a], Tianyang Chen[b], Jin-Hu Dou*[c], and Harish Banda*[a]

[a] Department of Chemistry and Biochemistry, The University of Texas at El Paso, El Paso, Texas, 79968, United States

[b] Department of Chemical Engineering, Stanford University, Stanford, California, 94305, United States

[c] School of Materials Science and Engineering, Peking University, Beijing, 100871, China

Corresponding Authors

* Jin-Hu Dou doujinhu@pku.edu.cn

* Harish Banda hbanda1@utep.edu

Table of Contents

Experimental Methods

Materials

All the precursors and salts used in this study were commercially available and used without further purification. Hydrated Copper Sulphate, Hydrated Copper Acetate, and Hydrated Copper Nitrate were procured from Sigma Aldrich. Methanol, Ammonium Acetate, and Acetic Acid were acquired from VWR. Acetonitrile, ethanol, and N.N-Dimethylformamide were obtained from Fisher Chemicals. Sulfolane was purchased from Thermo Scientific. 5,6 dimethoxy-benzo(c)isoxazole was custom-procured from Thesynnovator. Acetone was purchased from Macron Fine Chemicals. All electrolyte salts were procured from Sigma-Aldrich or Beantown Chemicals. In-house DI water was used during synthesis. Nitrogen gas was purchased from Syoxsa. 2,3,6,710,11-Hexahydroxytriphenylene (HHTP) was purchased from Thermos Scientific and Tertahydroxy-1,4-benzoquinone hydrate (THQ) was purchased from TCI chemicals.

Electrochemical characterization and analysis

All electrochemical measurements were carried out using a Biologic VSP-300 potentiostat. Cyclic voltammetry and Galvanostatic Cycling with Potential Limitation (GCPL) techniques were predominantly used for analysis. Experimental gravimetric capacity (Q_E) was calculated from the discharge sequence of three-electrode CV curves using Equation 1:

$$QE = (\int(iv)) * \frac{1000}{3600*2*mdv} \text{ (Equation 1)}$$

where $\int(iv) = \text{area of CV curve}$, m = mass of the MOF deposited as working electrode, *dv* = scan rate (mV/s). 3600 seconds and 1000 mA were used in the equation to convert the charge from Coulombs to mAh/g.

Theoretical capacities (Q_T in mAh/g) were calculated using Equation 2, where MW is the molecular weight of a MOF.

$$QT = (96500 * number\ of\ electrons) * \frac{1000}{3600*MW\ of\ MOF\ unit} \text{ (Equation 2)}$$

Electrochemical cell assembly

Working electrodes were prepared by hand coating MOF powders in the form of slurries on carbon paper (Fuel Cell-Toray Carbon Paper 060 Value Pack, Wet Proofed SKU#71070001). Slurries were prepared by repeatedly mixing a mixture of 80% MOF, 10% acetylene black, and 10% Polyvinylidene fluoride (PVDF) in DMF solvent. The slurry was applied on carbon paper (8mm diameter) and dried for 3 to 4 hours in the fume hood and then overnight in the oven at 60 ℃. These electrodes were used for all the experiments, except XPS. Activated carbon films were used as counter electrodes for all tests. Films were prepared by repeatedly mixing and kneading a mixture of 90% activated carbon, 5% acetylene black, and 5% Polytetrafluoroethylene solution (solution containing 60% PTFE and 40% Ethanol) in an ethanol solution. The films were dried overnight at 120 ℃. Activated carbon was purchased from MSE supplies (product code - SKU#: PO0198). It has a BET-specific surface area of 1670 m^2/g and a pore volume of 0.75 m^3/g. The mass of the counter electrode was taken 5 to 10 times larger than the working electrode to serve as an over-compensating electrode.

Custom-built T-shaped Swagelok cells fitted with stainless steel current collectors were used for electrochemical studies in three-electrode configurations. A leakless miniature Ag/AgCl electrode was used as the reference electrode whereas a paper served as the separator. Two electrode coin cells (Digital pictures of the Swagelok cell and the coin cell setups used for electrochemical studies in this work. Swagelok cell enabled tests in three-electrode configuration and typically accommodates ~2 ml of electrolyte. Coin cell setup uses a relatively small amount of electrolyte (50 microliters).) were assembled under dry and oxygen-free conditions using a Nitrogen-filled glove box with O_2 and H_2O levels < 1 ppm. A Whatman GF/B glass microfiber filter (CAT No. 1821-047) was used as a separator.

Electrochemical Quartz Crystal Microbalance (EQCM)

All the EQCM experiments were performed using Stanford Research Systems – Model QCM-200. 5 MHz gold-coated crystals brought from Fil-Tech were used as the substrates to be prepared as working electrodes. Working electrodes were prepared by drop-casting a suspension of MOF powders. Suspensions were prepared in Eppendorf tubes by mixing 2mg of Cu_3HHTT_2 MOF (60%

by mass), 1mg of acetylene black (30% by mass), and 0.33mg of Polyvinylidene fluoride (PVDF-10% by mass) in 0.5ml of DMF. The mixture was sonicated for 30 minutes to mix the mixture uniformly. Five microliters of this suspension (approximately 20 micrograms by weight) were deposited on the gold crystal. The crystals were dried overnight at 60 °C. Suspensions were prepared in Eppendorf tubes by mixing 2mg of Cu_3HTHQ_2 MOF (60% by mass), 1mg of acetylene black (30% by mass), and 0.33mg of Polyvinylidene fluoride (PVDF-10% by mass) in 0.5ml of DMF. The mixture was sonicated for 30 minutes to mix the mixture uniformly. Five microliters of this suspension (approximately 20 micrograms by weight) were deposited on the gold crystal. The crystals were dried overnight at 60 °C.

Instrumental Methods

Powder X-ray diffraction (PXRD) measurements were performed on a p-XRD Empyrean 2 PANanalytical diffractometer with a Cu Kα (λ = 1.5418 A^o) radiation source equipped with a θ/2θ Bragg-Brentano geometry (Kα1 = 1.5406 Å, Kα2 = 1.5444 Å, Kα2/Kα1 = 0.5). The generator voltage and tube current were 45 kV and 40 mA, respectively. The scanning range is from 1.2° to 40°, with a step size of 0.01313°. Each step had a duration of 48.195 seconds. PXRD data of the electrodes were recorded by placing a piece of carbon paper coated with electrode material on a zero-background silicon crystal plate.

Scanning Electron Microscopy (SEM) images were obtained using the Hitachi-4800 scanning electron microscope. SPI sputter coating module was used to coat gold over the pellets for improved imaging.

X-ray photoelectron Spectroscopy (XPS) spectra were collected using a ThermoFisher Nexsa G2 X-ray photoelectron spectrometer with an Al source. The scans were recorded using a 400-um spot size with a flood gun to correct any charge effect. The survey scans were collected using a fixed pass energy of 200 eV and an energy step size of 1 eV for a total of 1361 steps. The high-res scan used a fixed pass energy of 50.0 eV and an energy step of 0.100 eV, the total number of steps depends on the size of the window for each element. CASA software was used for processing and analysis of the data and samples as well as identification of the peaks (Figure 1d,1e, and Figure S3). BE calibration was carried out by shifting the C1s peak of the C-C bond position 284.8 eV

(Source: Thermo Scientific). Samples for *ex-situ* XPS are prepared as thin films. MOF films were prepared by repeatedly mixing and kneading a mixture of 60% MOF powder, 30% acetylene black, and 10% Polytetrafluoroethylene solution (solution containing 60% PTFE and 40% Ethanol) in an ethanol solution. The film was dried overnight at 60 ℃. Three electrode cells were first cycled at a scan rate of 2 mV/s for 2 cycles and then held at a constant potential of –0.750 or -0.150 V vs. Ag/AgCl for 1 hour till the residual currents were less than 50 uA. Cells were then disassembled, and the polarized electrodes were carefully handled to perform XPS analyses.

Inductively coupled plasma mass spectrometry (ICP-MS) was performed by Robertson Microlit, a service provider for analytical techniques. Electrolytes retrieved from the cycled and degraded cells were diluted to 6 ml and shipped for analysis.

UV–vis absorption spectra were measured between wavelengths of the range 200–600 nm. All observations were recorded using the Chemglass Life Sciences SpecMate spectrophotometer.

The solubility of the ligands was estimated by dissolving known amounts of solids into water and ACN. The solutions were sonicated for an hour, heated at 50 °C, and filtered using a paper with 0.25 um pores. The solids were weighed, and the obtained masses were used to calculate the solubilities of the ligands.

Synthesis

Synthesis of 2,3,7,8,12,13-Hexahydroxytricycloquinazoline (HHTT)[1]

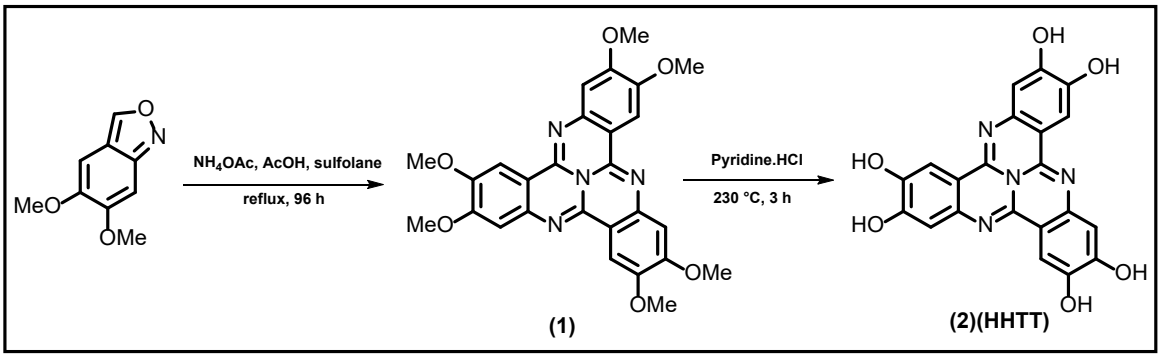

Synthesis of 2,3,7,8,12,13-Hexamethoxytricycloquinazoline (1)

To a mixture of sulfolane (100 mL) and glacial acetic acid (25 mL) was added ammonium acetate (12 g, 156 mmol) and 5,6-dimethyoxyanthranil 2 (4 g, 22.33 mmol). The reaction mixture was refluxed for 96 hours and cooled down to room temperature, after which water was added. The resulting greenish-yellow solid was collected by suction filtration, washed with water and methanol, and dried under air to give 820 mg.

Synthesis of 2,3,7,8,12,13-Hexahydroxytricycloquinazoline (HHTT) (2)

A mixture of 2,3,7,8,12,13-hexamethoxytricycloquinazoline 3 (800 mg, 1.6 mmol) and pyridine hydrochloride (27 g, 234 mmol) was heated to 240 °C for 3 hours and then cooled down to room temperature. Water was then added to the mixture, and the resultant black precipitate was collected by suction filtration, washed with water, and dried under vacuum to yield 320 mg (50%) of 2,3,7,8,12,13-hexamethoxytricycloquinazoline (HHTT). ^{1}H NMR (400MHz, DMSO-d6): δ = 10.06 (3H), 9.64 (3H), 7.58 (3H), 6.72 (3H) ppm.

Synthesis of Cu_3HHTT_2 MOF[2]

A solution of 12.0 mg (0.05 mmol) of copper nitrate trihydrate ($Cu(NO_3)_2{\cdot}3H_2O$) in 6 mL of water was added to a solution of 33.28 mg (0.08 mmol) of HHTT in 2 mL of dimethylformamide (DMF). This mixture was treated with ultrasonication in a vial for 10 min and thereafter placed in an 85 °C

oven for 72 h. The resulting black powder was centrifuged and washed with water and acetone several times and then dried overnight at 60 °C.

Synthesis of Cu_3HHTP_2 MOF[3]

$Cu(CH_3COO)_2 \cdot H_2O$ (63 mg) and 2,3,6,7,10,11-hexahydroxytriphenylene (HHTP, 194.4 mg) were weighed and placed in a 50 mL glass vial. Then the 30 mL mixture solution of DMF and H_2O was added with a volume ratio of 1:1. The whole solution was stirred and dissolved. Then the glass vial was placed in the oven and heated to 85 °C for 12 h. When the above reaction is completed, the dark blue product can be obtained after centrifugation with ethanol and drying.

Synthesis of Cu_3THQ_2 MOF[4]

$Cu(NO_3)_2 \cdot 2.5H_2O$ (798 mg, 3.44 mmol) was dissolved in 150 mL degassed H_2O under N_2 protection. Then subsequently, ethylenediamine (0.35 mL, 5.25 mmol) was added. In a separate flask, tetrahydroxyquinone (THQ) (300 mg, 1.74 mmol) was dissolved in 150 mL degassed H_2O and then transferred via cannula to the copper solution under vigorous stirring. The reaction was further stirred at 500 rpm for 12 h at RT under the N_2. The dark navy precipitate was obtained and filtered. The product was subsequently washed with H_2O (100 mL × 2) and acetone (50 mL × 2) and dried in a 60 °C oven for further characterization.

EQCM Calibration

Although EQCM can be reliably used in liquid solutions, the viscous loading on one side of the crystal requires re-calibration of the conversion factor for the Sauerbrey equation:

$$\Delta f = -C_f \Delta m$$

The gold crystal used has C_f = 56.6 Hz cm^2 μg^{-1} in the air with a gold coating surface area of 1.22 cm^2. The mass change in aqueous electrolytes was calibrated according to the protocol described in the SRS QCM200 manual. Silver was deposited and stripped from an aqueous solution of 0.05 M AgNO3 (Alfa Aesar) in 0.5 M HNO3 (Fisher Scientific) onto a new crystal at 100µA. The linear changes in frequency are shown in (Frequency changes during the deposition of Silver from a solution of 50 mM AgNO3 in 0.5 M HNO3 in water. An average of the slopes from the three curves above is used to convert Δf to Δm.). We then used the following equation to calculate the equivalent C_f (Hz/microgram) for 100 µA current[5].

Current (µA)	**Current density (Current/Area in cm^2)**	**Slope (delta f/t)**	**C_f (Hz/µg)**	**1/C_f (µg/Hz)**	**Mass Loss (1/C_f)*delta f**
100	81.9	1.87	20.41	0.048	5.6 µg
100	81.9	1.92	20.99	0.047	5.4 µg
100	81.9	2.01	21.94	0.045	5.2 µg

$$C_f = \frac{-n \cdot F \cdot \Delta f}{M_{Ag} \Delta Q}$$

n = # of electrons transferred [mol e^- /mol Ag or other depositing species], F = 96485 C mol^{-1} e^-

Δf = change in frequency during deposition, M_{Ag} = 107.86 g/mole, molecular mass of silver [g/mol]

ΔQ = charge passed during deposition

Values from 3 trials were averaged to obtain C_f 21 Hz/ug or 1/ C_f as 46.6 ng/Hz. Applying these values to three trials on Cu_3THQ_2 MOF, with an average delta frequency of 115 Hz, gave an average mass loss of 5.5 ug.

In air, the change in frequency of the crystal used for deposition was 4362 Hz or 0.08% of the unloaded crystal's resonance frequency. Also, when immersed in a liquid, the undeposited crystal experiences a frequency drop of 896 Hz. Relative to a theoretical drop of 715 Hz for a crystal going from vacuum to liquid, this is a reasonable change in frequency.

Formula unit	Mass (g)	Theoretical capacity for $1e^-$ reduction (mAh/g)	Theoretical capacity for $2e^-$ reduction (mAh/g)	Theoretical capacity for $3e^-$ reduction (mAh/g)	Theoretical capacity for $4e^-$ reduction (mAh/g)
Cu_3HHTT_2	1011.238	26.5	53	79.51	106.01
Cu_3HHTP_2	827.118	32.4	64.81	97.21	129.61
Cu_3THQ_2	526.758	50.88	101.76	152.64	203.52

Table S1. Theoretical capacity calculations for the three MOFs studied in this work.

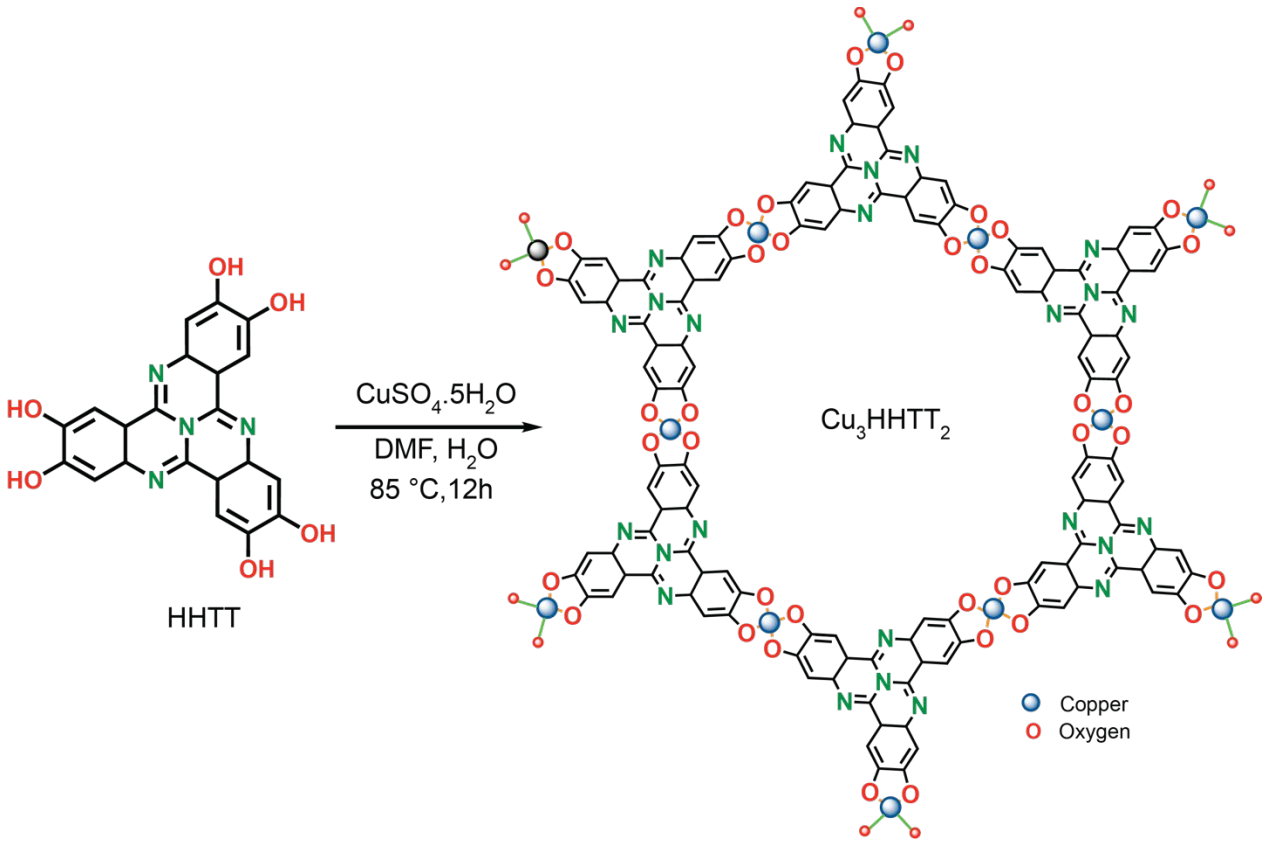

Scheme 1. Schematic depicting the synthesis of Cu_3HHTT_2 using HHTT ligand. The obtained product was washed sequentially with copious amounts of deionized water, DMF, ethanol, and acetone.

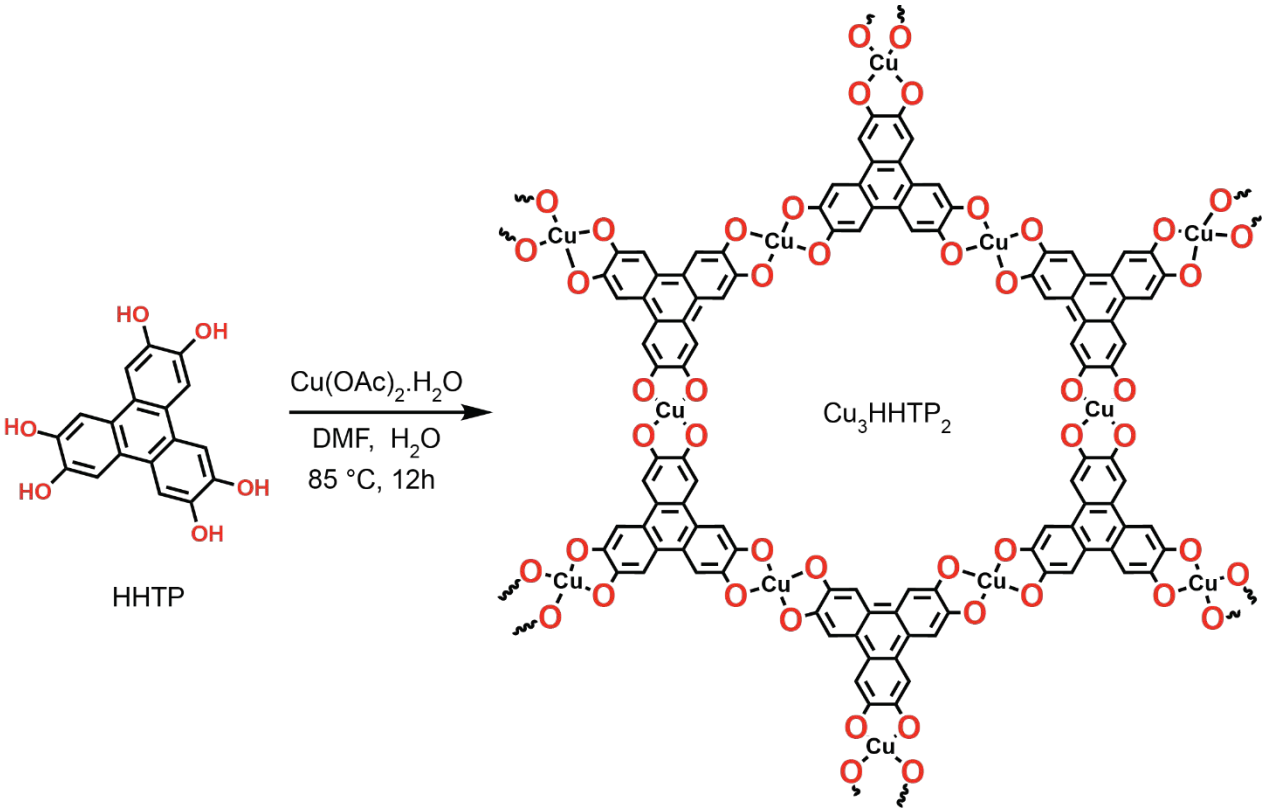

Scheme 2. Schematic depicting the synthesis of Cu_3HHTP_2 using HHTP ligand. The obtained product was subsequently washed with copious amounts of deionized water, DMF, ethanol, and acetone.

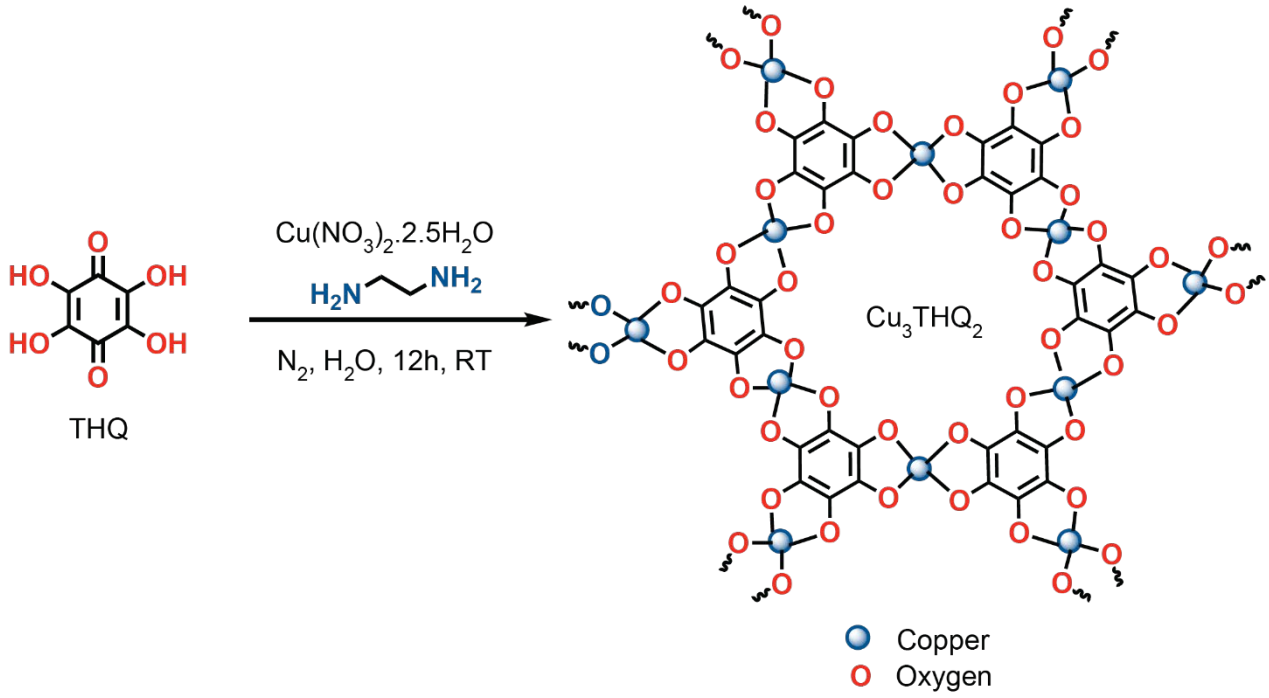

Scheme 3. Schematic depicting the synthesis of Cu_3THQ_2 using THQ ligand. The obtained product was washed sequentially with copious amounts of deionized water, DMSO, ethanol, and acetone.

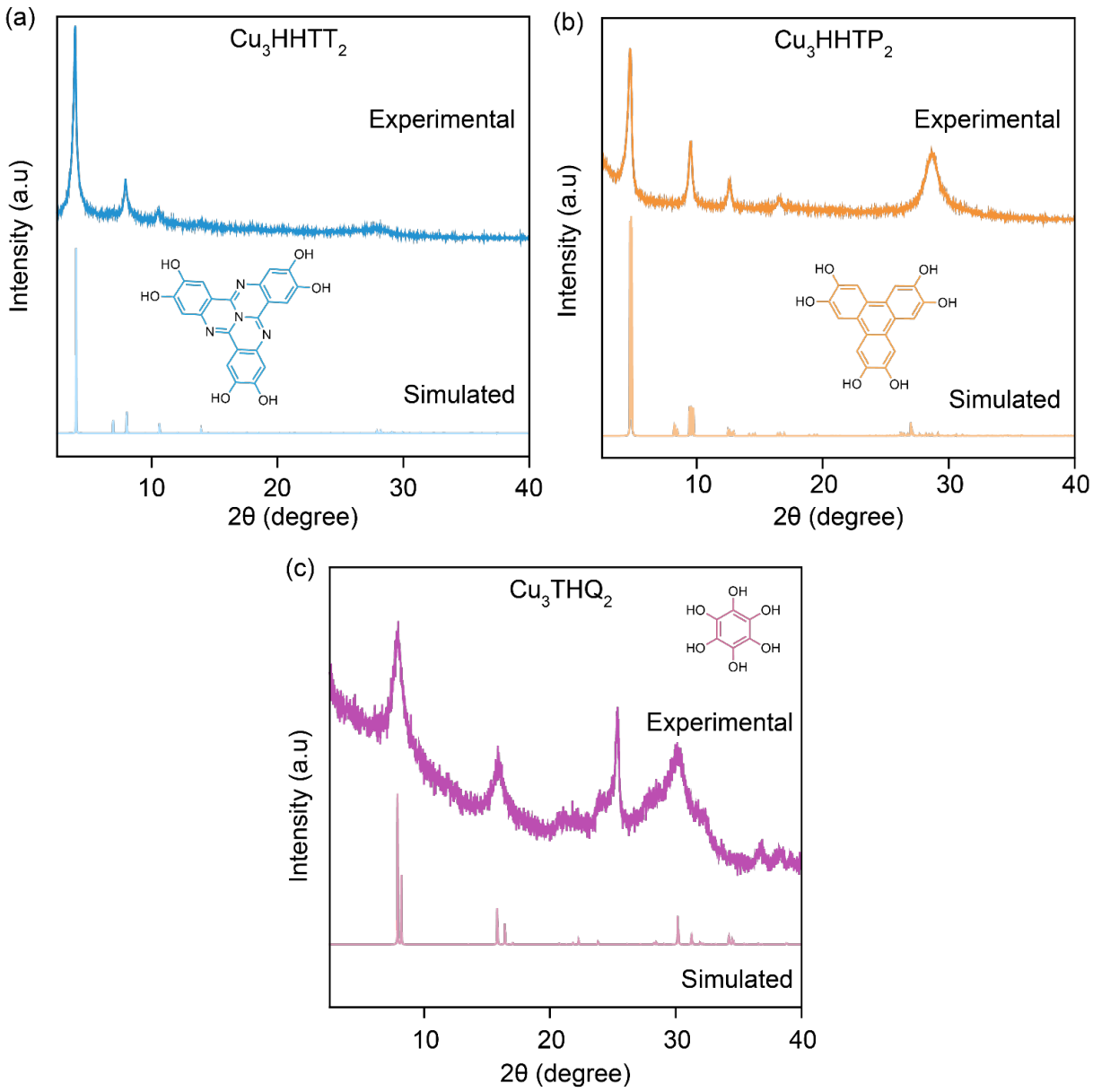

Figure S1. Experimental and simulated PXRD patterns for (a) Cu_3HHTT_2, (b) Cu_3HHTP_2, and (c) Cu_3THQ_2.

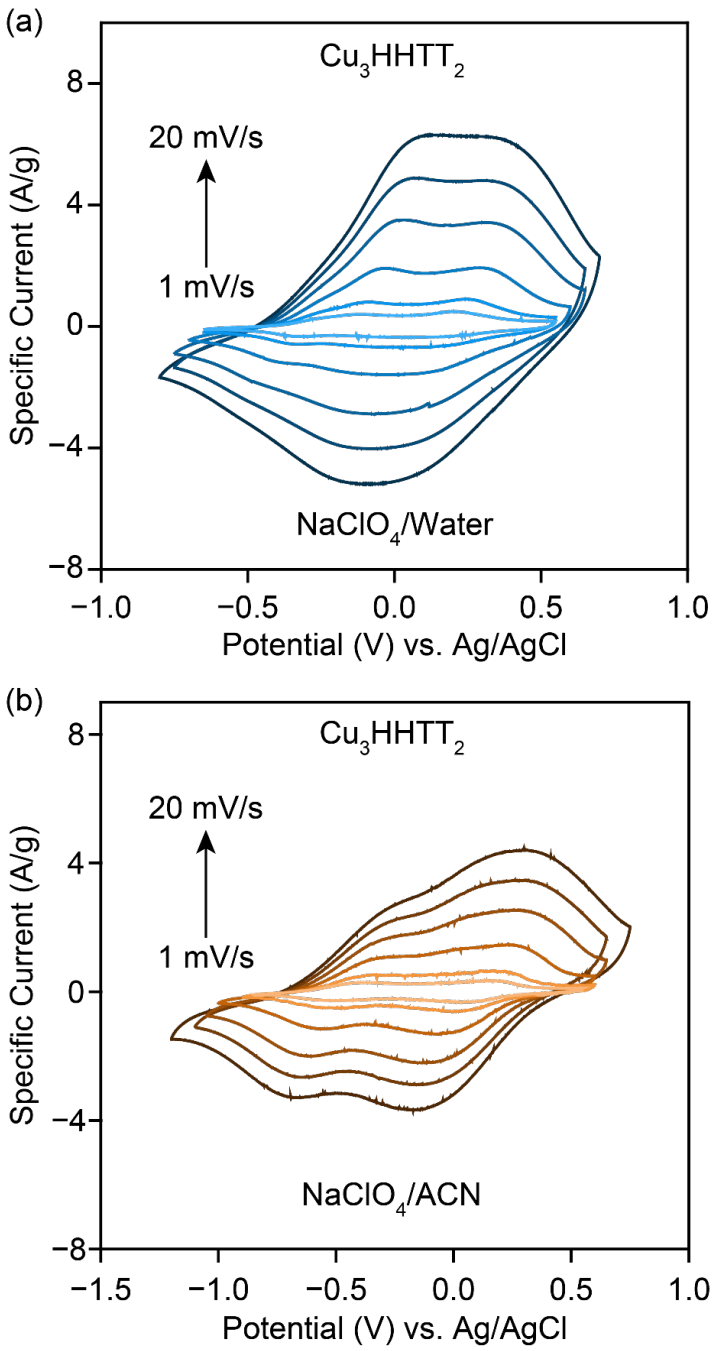

Figure S2. Cyclic voltammetry of Cu_3HHTT_2 MOF at various scan rates from 20 mV/s to 1 mV/s in 0.5 M $NaClO_4$/water and $NaClO_4$/ACN electrolytes.

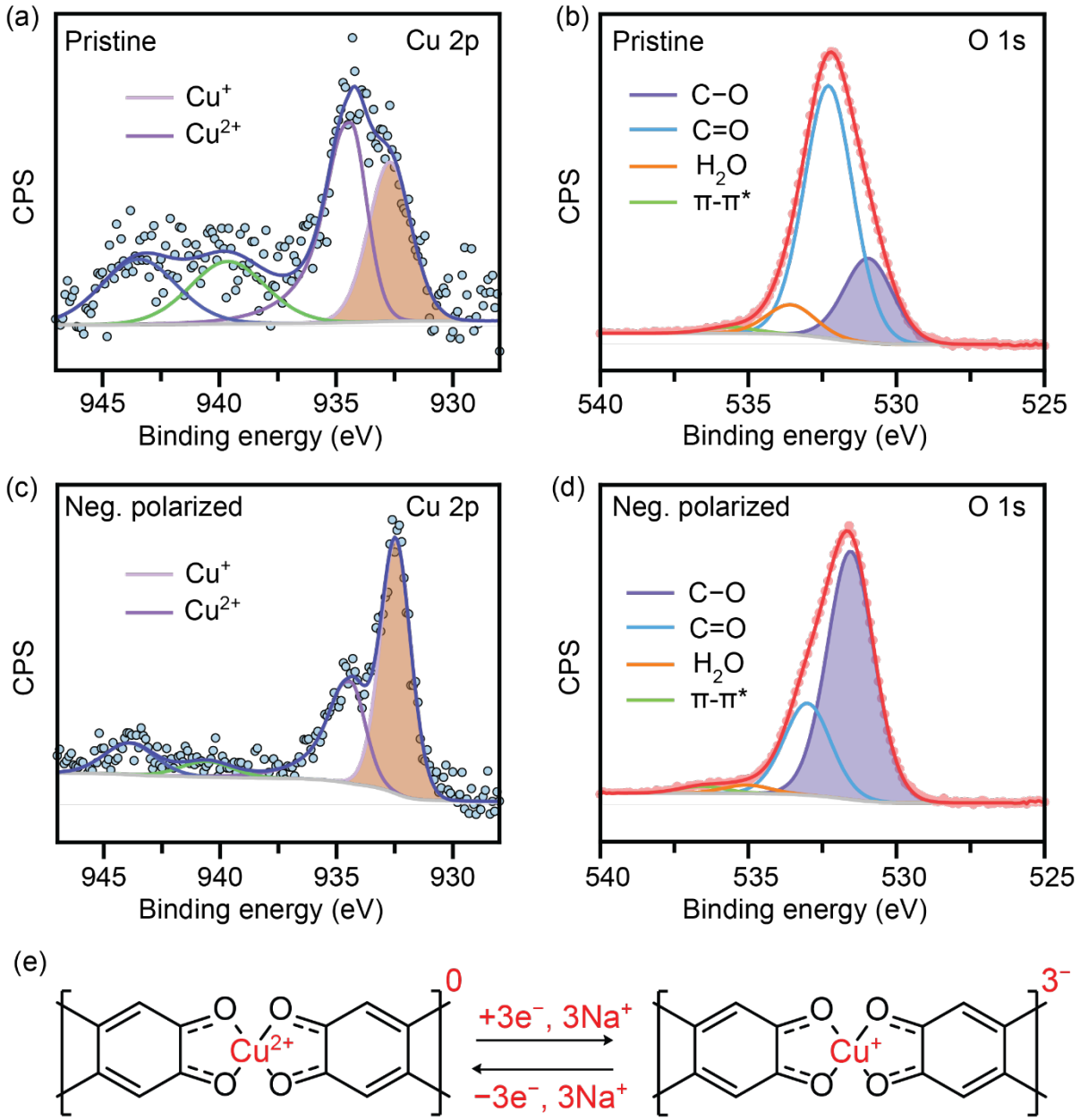

Figure S3. High resolution (HR) (a, c) Cu 2p and (b, d) O 1s XPS spectra of (a, b) pristine and (c, d) negatively polarized (−0.75 V vs. Ag/AgCl) samples of Cu_3HHTT_2. Clear changes, attributed to the reduction of copper and ligand, are observed from Cu 2p and O 1s HR spectra. (e) Schematic indicating the three-electron reduction of Cu_3HHTT_2.

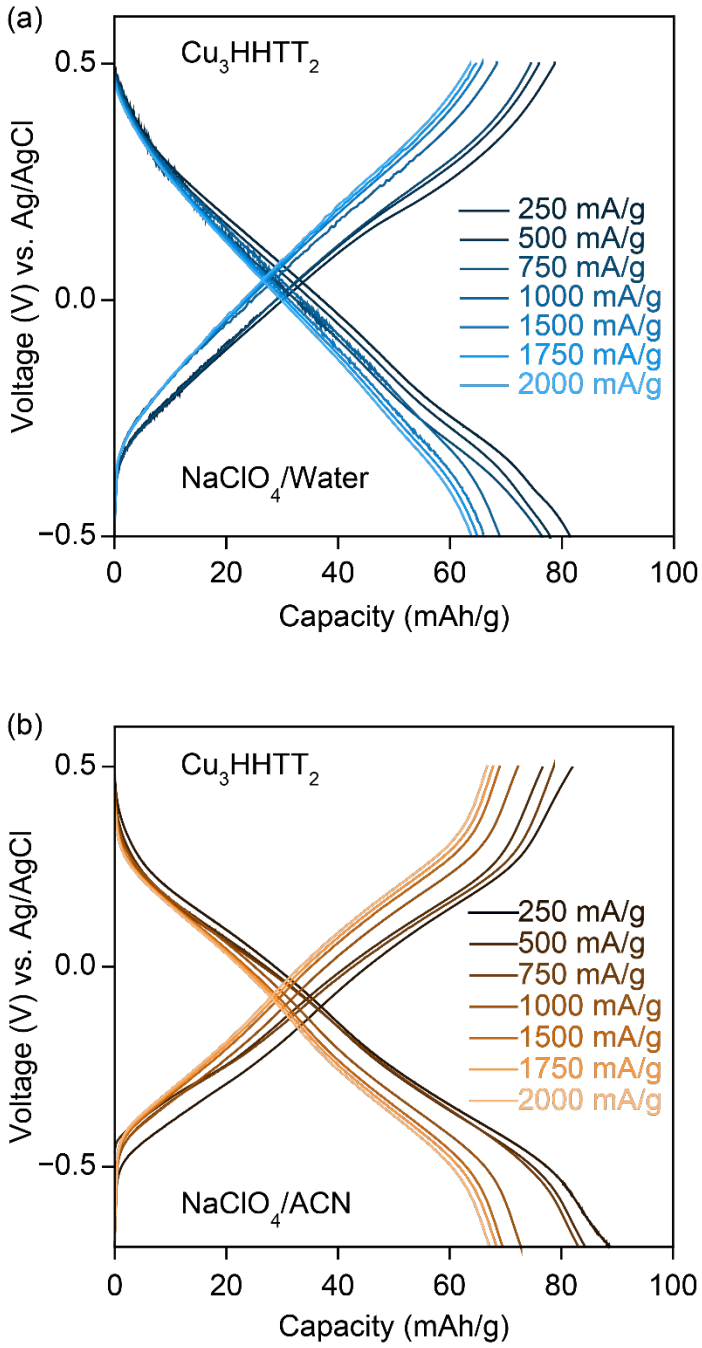

Figure S4. GCPL voltage profiles of Cu_3HHTT_2 at various current densities from 250 mA/g to 2000 mA/g using (a) 0.5 M $NaClO_4$/water and (b) $NaClO_4$/ACN electrolytes.

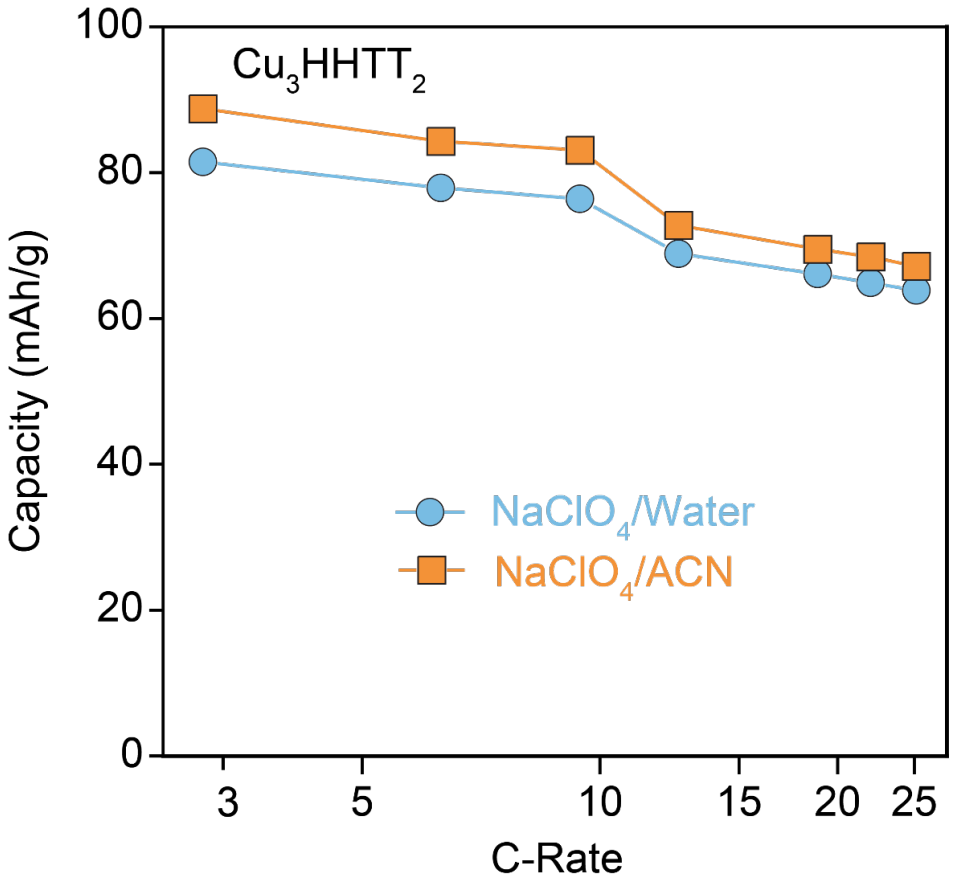

Figure S5. The power capability of Cu_3HHTT_2 was recorded in GCPL tests using current densities ranging from 250 mA/g (3C) to 2000 mA/g (25C) using 0.5 M $NaClO_4$/water and $NaClO_4$/ACN electrolytes.

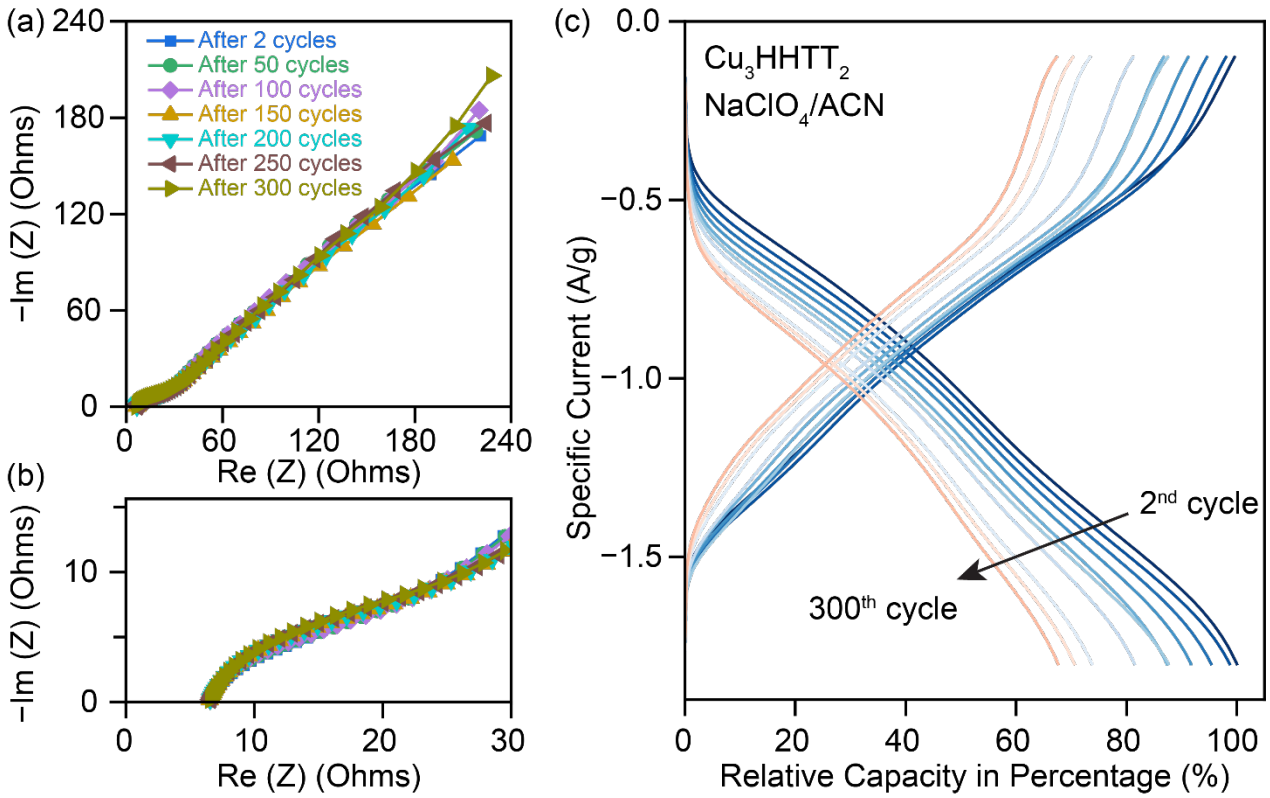

Figure S6. (a) Nyquist plots of potentiostatic electrochemical impedance for Cu_3HHTT_2 were recorded after every 50 cycles of GCPL cycling at a current density of 750 mA/g in non-aqueous $NaClO_4$ electrolyte (acetonitrile). Frequencies ranging from 200 kHz to 100 mHz are used. (b) Zoomed response of (a). (c) The corresponding Charge-discharge GCPL profiles of Cu_3HHTT_2 depict a capacity loss of ~35% over 300 cycles. Impedance responses remain largely unaffected despite the notable capacity losses.

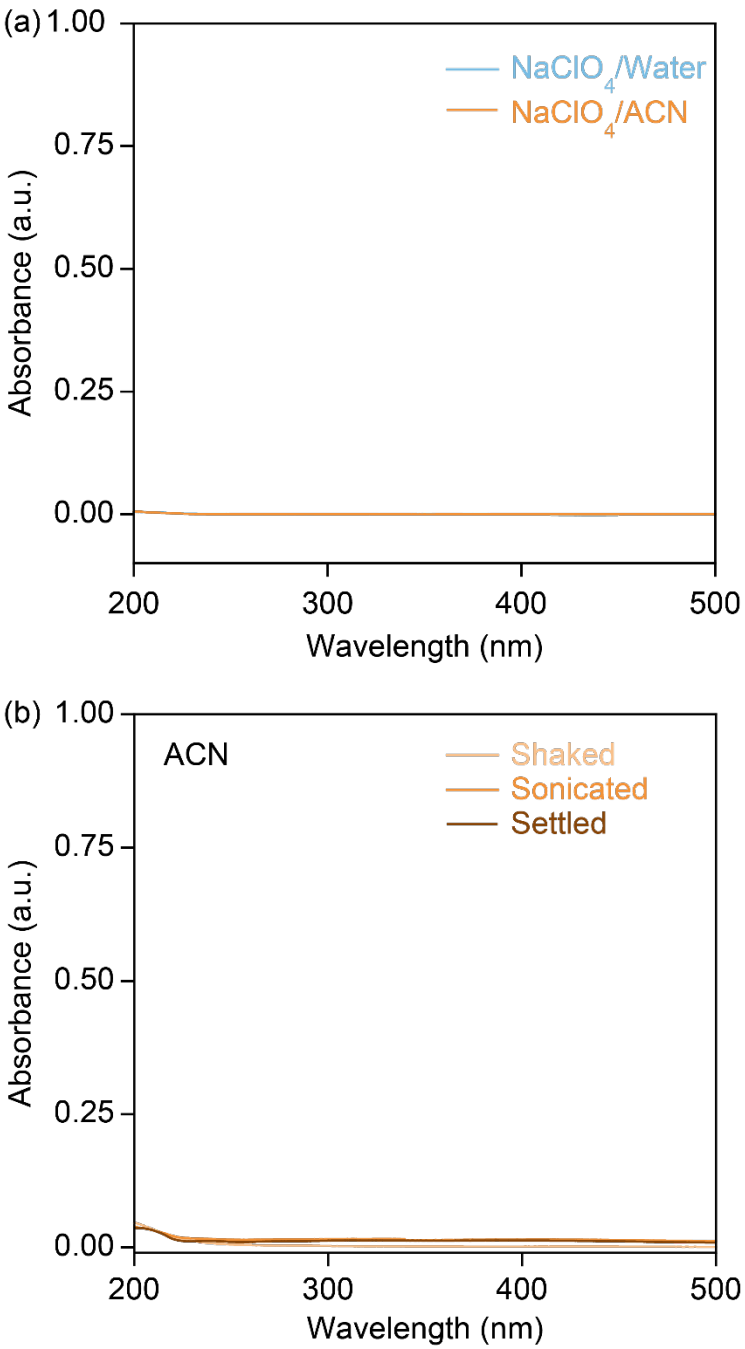

Figure S7. (a) UV-Vis spectra of 0.5 M $NaClO_4$/water and $NaClO_4$/ACN electrolytes. (b) UV-Vis spectra of the colloidal solutions were prepared by mixing 1 mg of Cu_3HHTT_2 MOF into 3 ml of ACN. Spectra were recorded after vigorously shaking, sonicating the mixture for 1 minute, and letting the sonicated solution rest for one hour. All three spectra indicate minimal presence of Copper or HHTT.

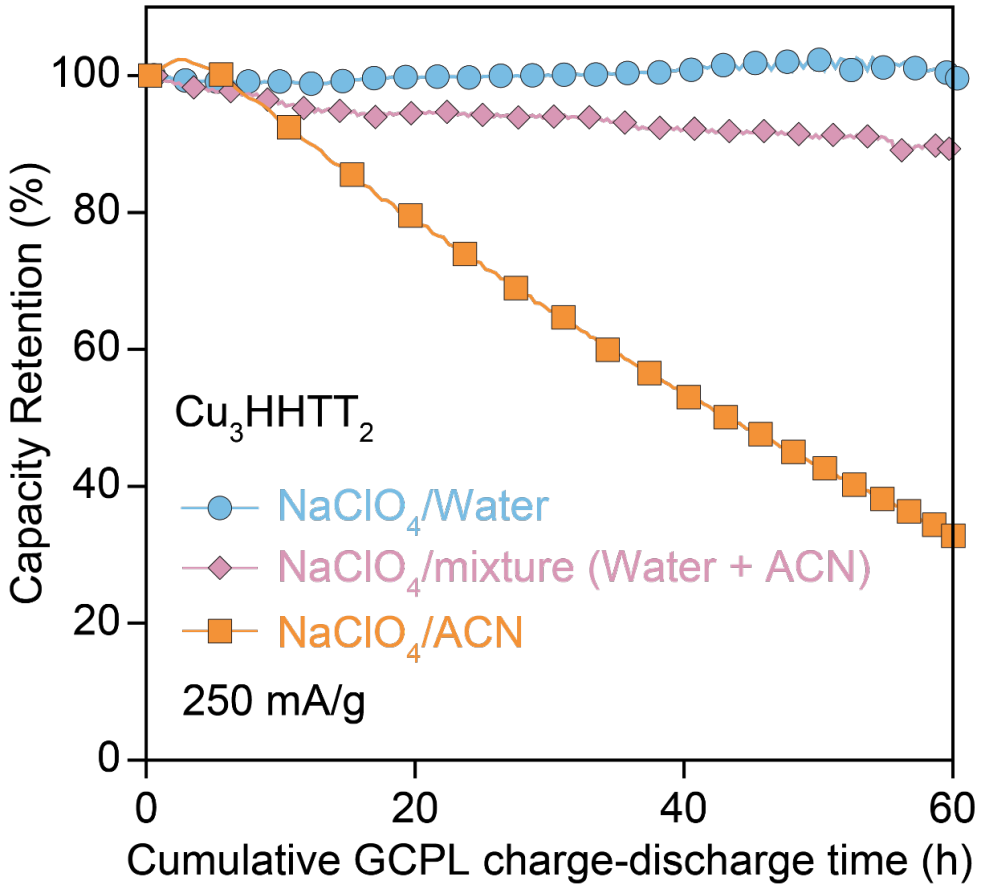

Figure S8. Capacity retention plots of Cu_3HHTT_2 during GCPL cycling at a current density of 250 mA/g in three different electrolytes – 0.5 M $NaClO_4$/water, $NaClO_4$/ACN, and $NaClO_4$/(1:1 water + ACN) electrolytes.

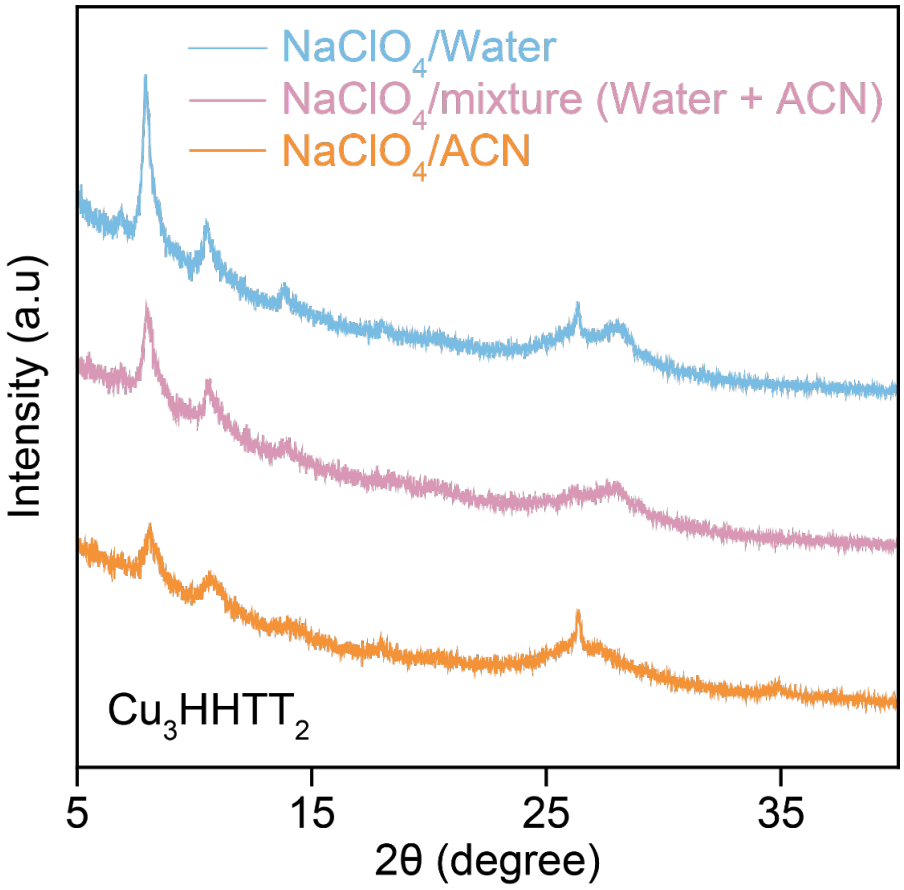

Figure S9. Powder X-ray diffraction patterns of Cu_3HHTT_2 electrodes after GCPL cycling for 60 hours at a current density of 250 mA/g in three different electrolytes -0.5 M $NaClO_4$/Water, $NaClO_4$/ACN, and $NaClO_4$/(1:1 Water + ACN) electrolytes. An additional peak at ~26° in the electrodes corresponds to the carbon paper substrate.

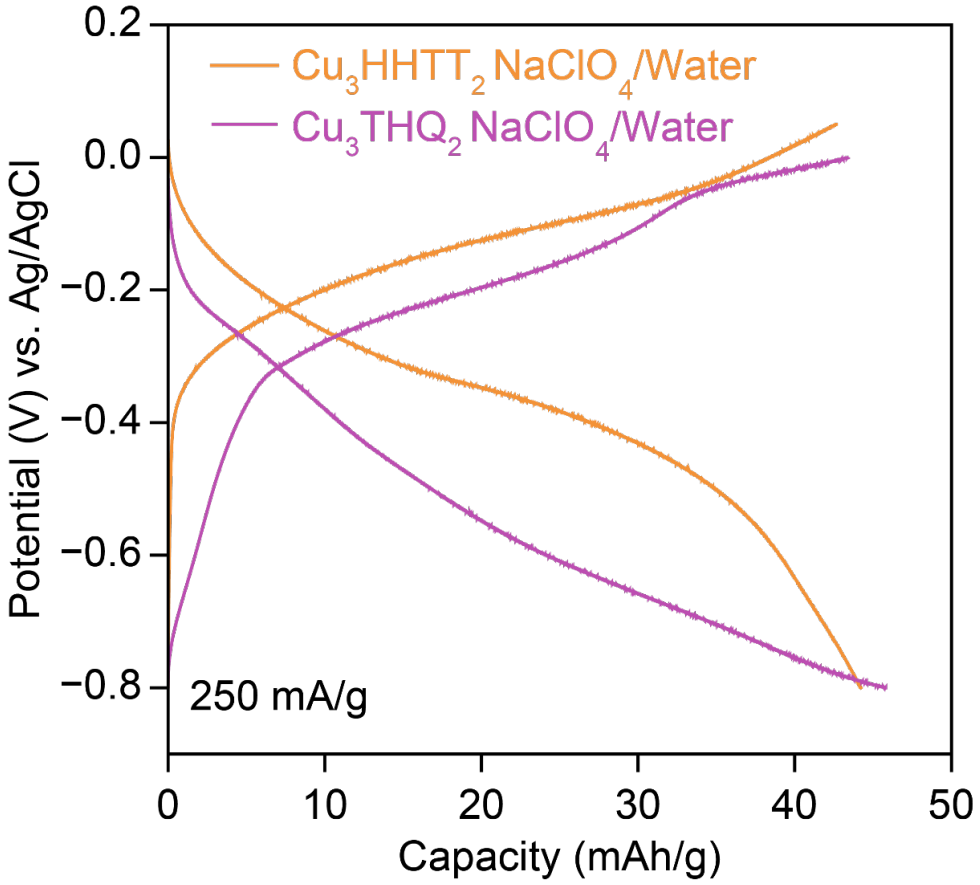

Figure S10. GCPL voltage profiles of Cu_3HHTP_2 and Cu_3THQ_2 at a current density of 250 mA/g using 0.5 M $NaClO_4$/Water as the electrolyte.

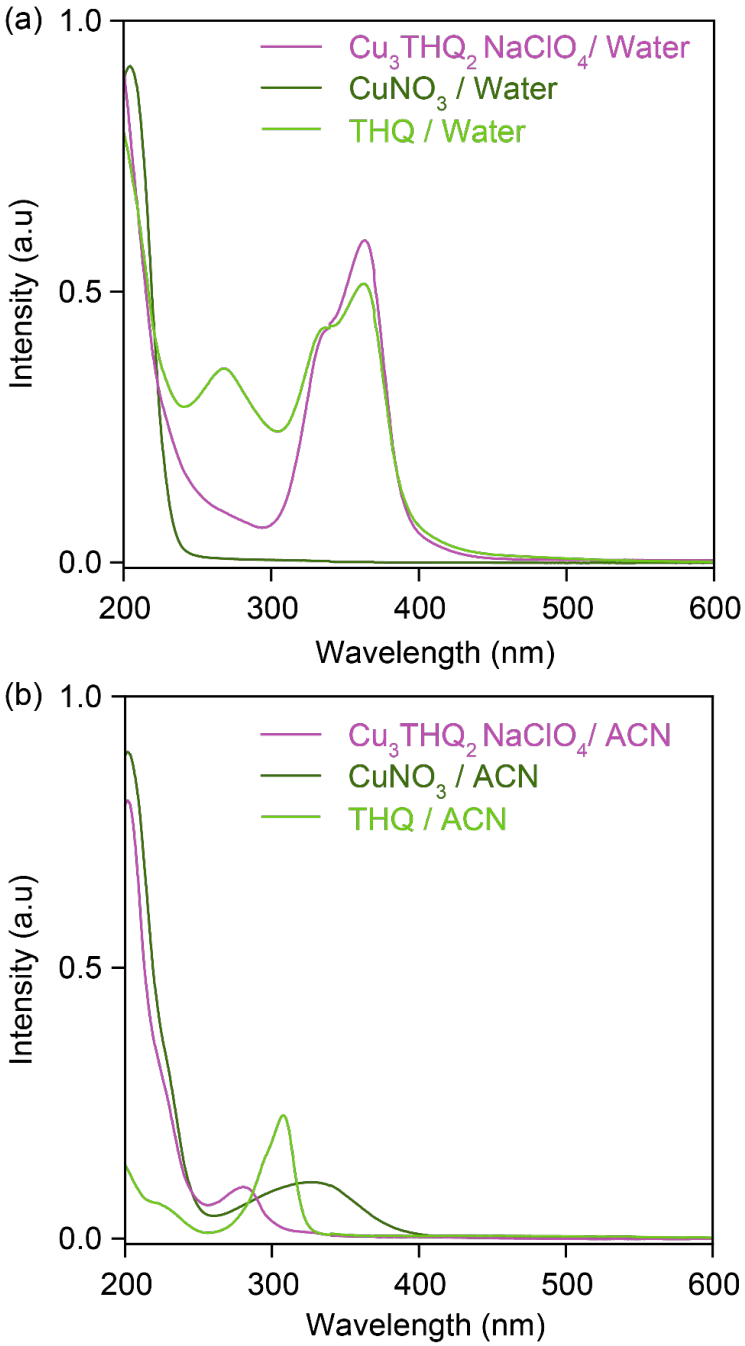

Figure S11. UV-Vis spectra of an electrolyte retrieved after cycling an electrode of Cu_3THQ_2 in (a) 0.5 M $NaClO_4$/Water and (b) 0.5 M $NaClO_4$/ACN. UV-Vis spectra of Copper Nitrate, and Tetrahydroxyquinone (THQ) are also shown.

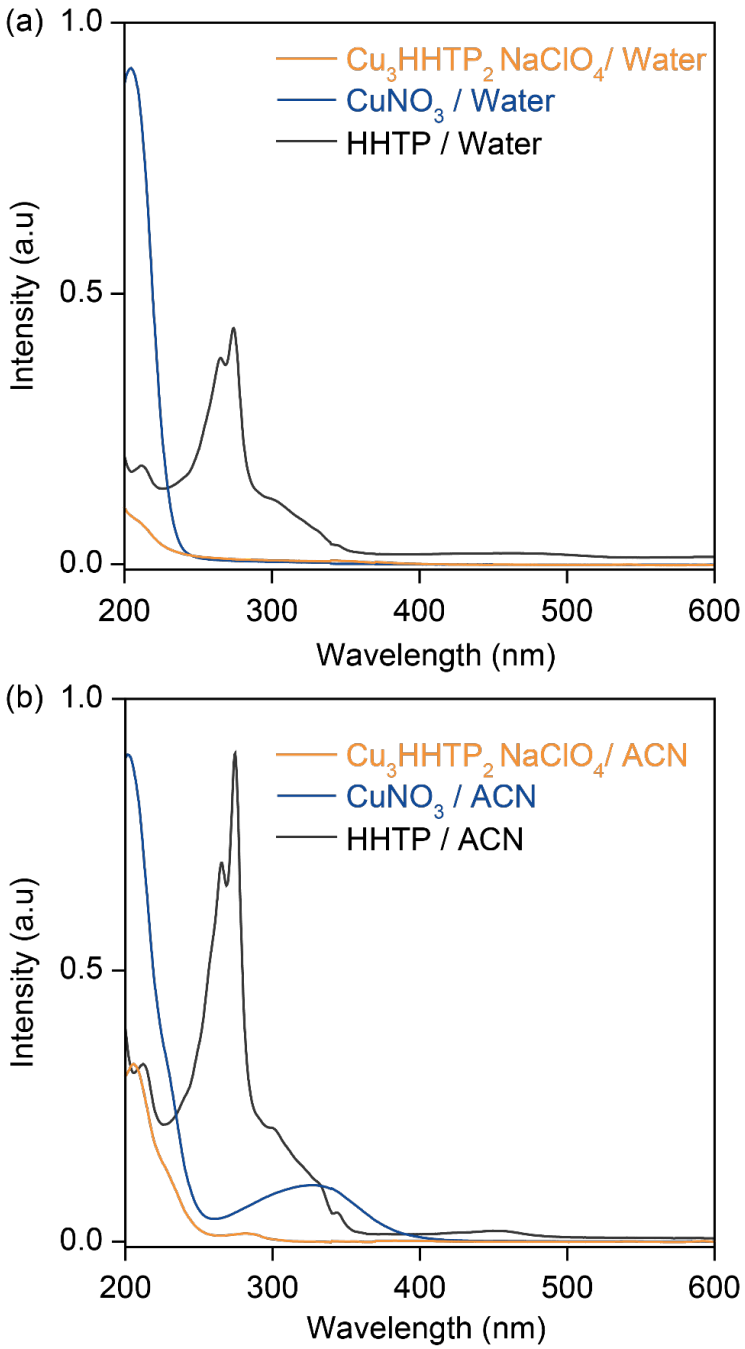

Figure S12. UV-Vis spectra of an electrolyte retrieved after cycling an electrode of Cu_3HHTP_2 in (a) 0.5 M $NaClO_4$/Water and (b) $NaClO_4$/ACN. UV-Vis spectra of Copper Nitrate, and Hexahydrotriphenylene (HHTP) are also shown.

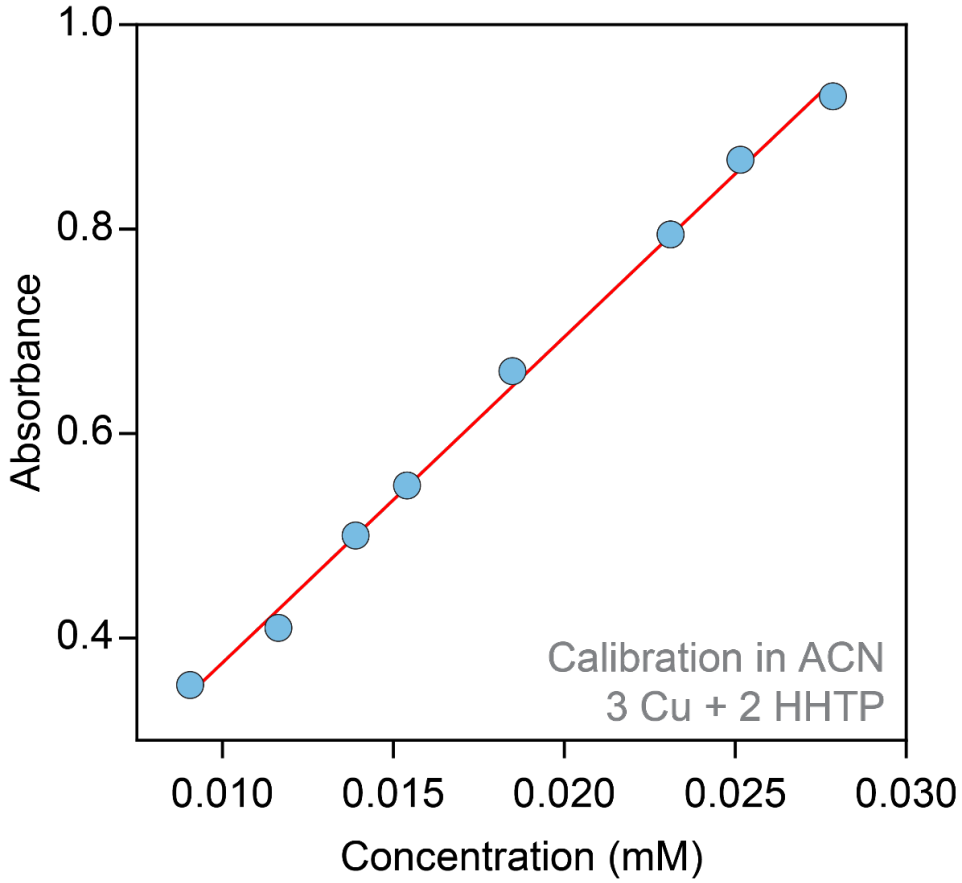

Figure S13. A calibration curve for acetonitrile solutions containing Copper Nitrate and HHTP in a ratio of 3:2 was used along with Beer-Lambert's law. The slope from this curve is used to calculate the concentration of Cu_3HHTP_2 present in the electrolyte.

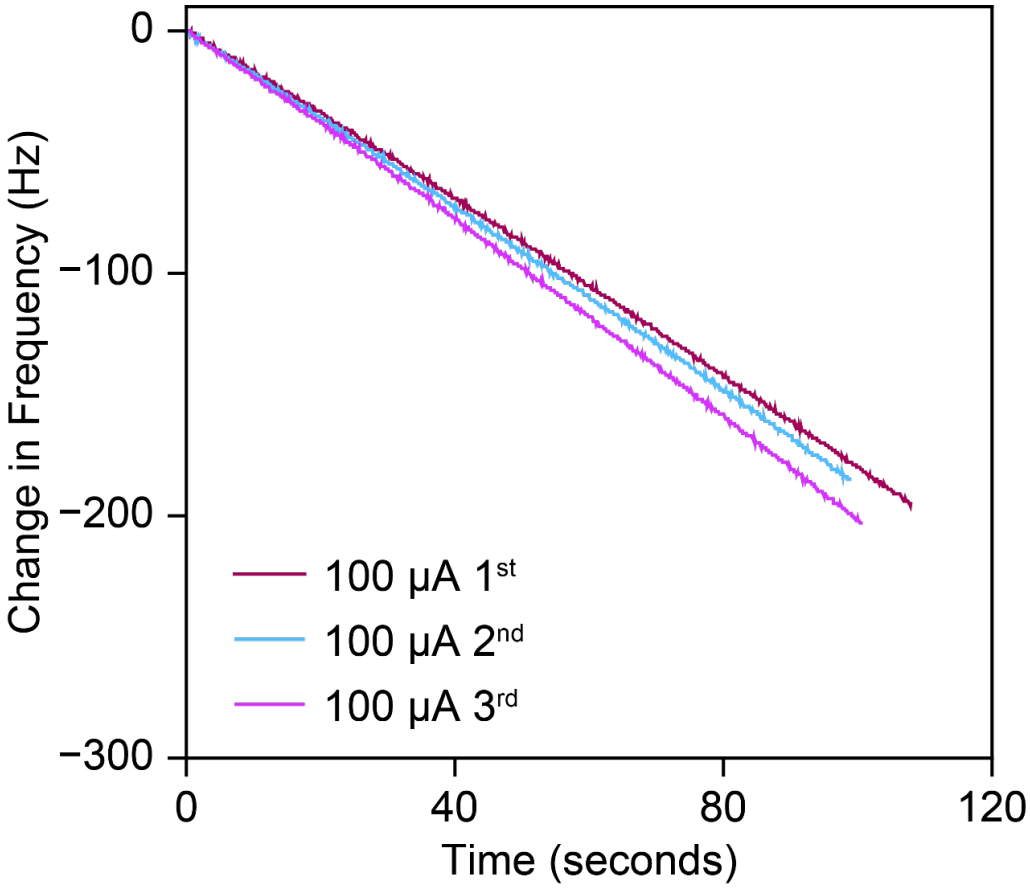

Figure S14. Frequency changes during the deposition of Silver from a solution of 50 mM $AgNO_3$ in 0.5 M HNO_3 in water. An average of the slopes from the three curves above is used to convert Δf to Δm.

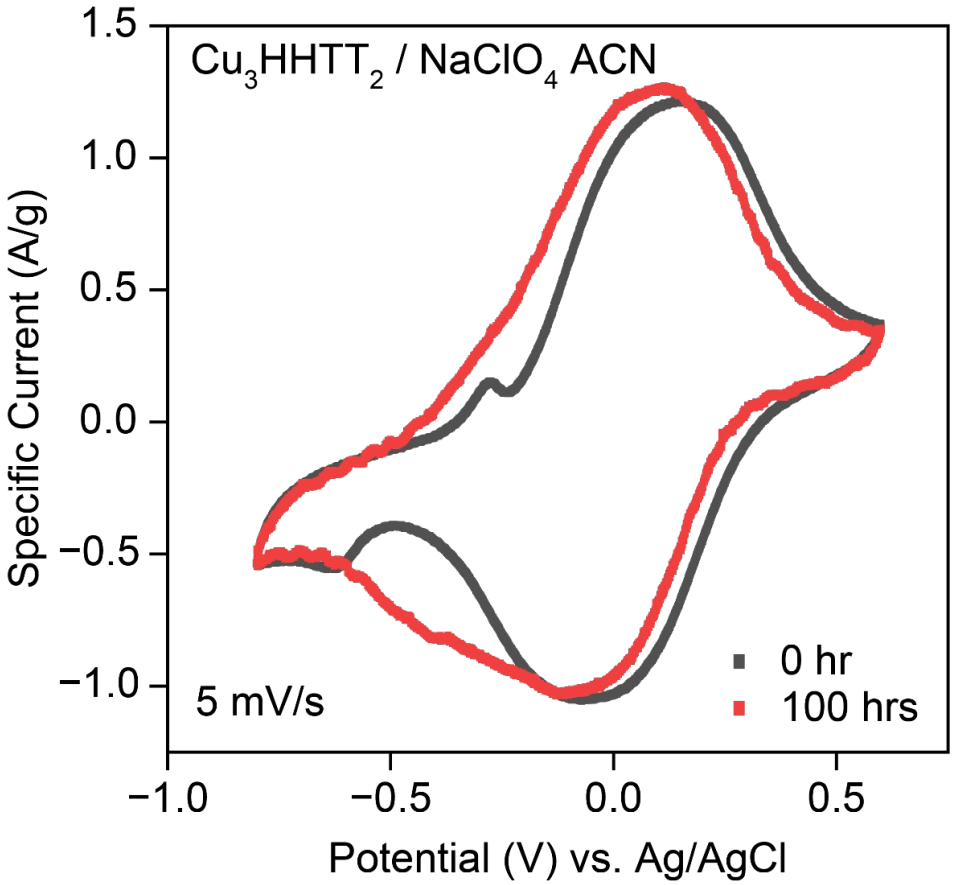

Figure S15. Cyclic voltammetry of Cu_3HHTT_2 was recorded at a scan rate of 5 mV/s in $NaClO_4$/ACN immediately after cell assembly and after 100 hours of rest.

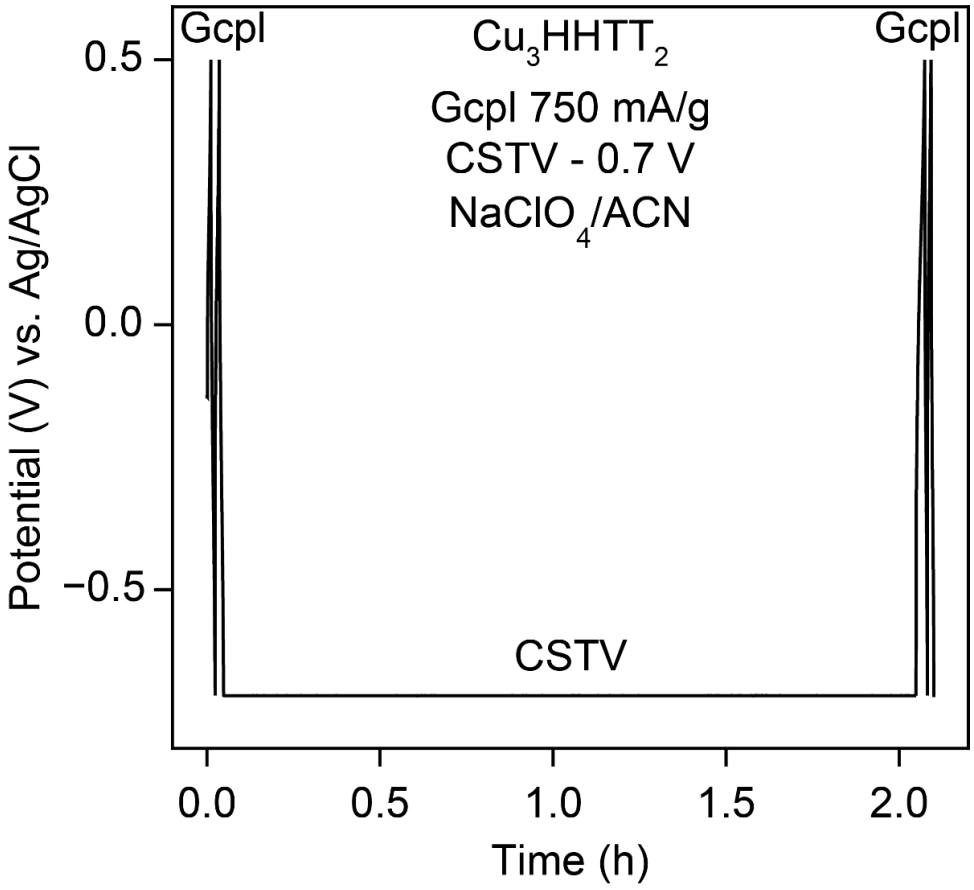

Figure S16. Potential versus time profile corresponding to GCPL plus constant potential (CSTV) electrochemical tests done on Cu_3HHTT_2 using $NaClO_4$/ACN. Capacities plotted from these tests are shown in Figure 6a.

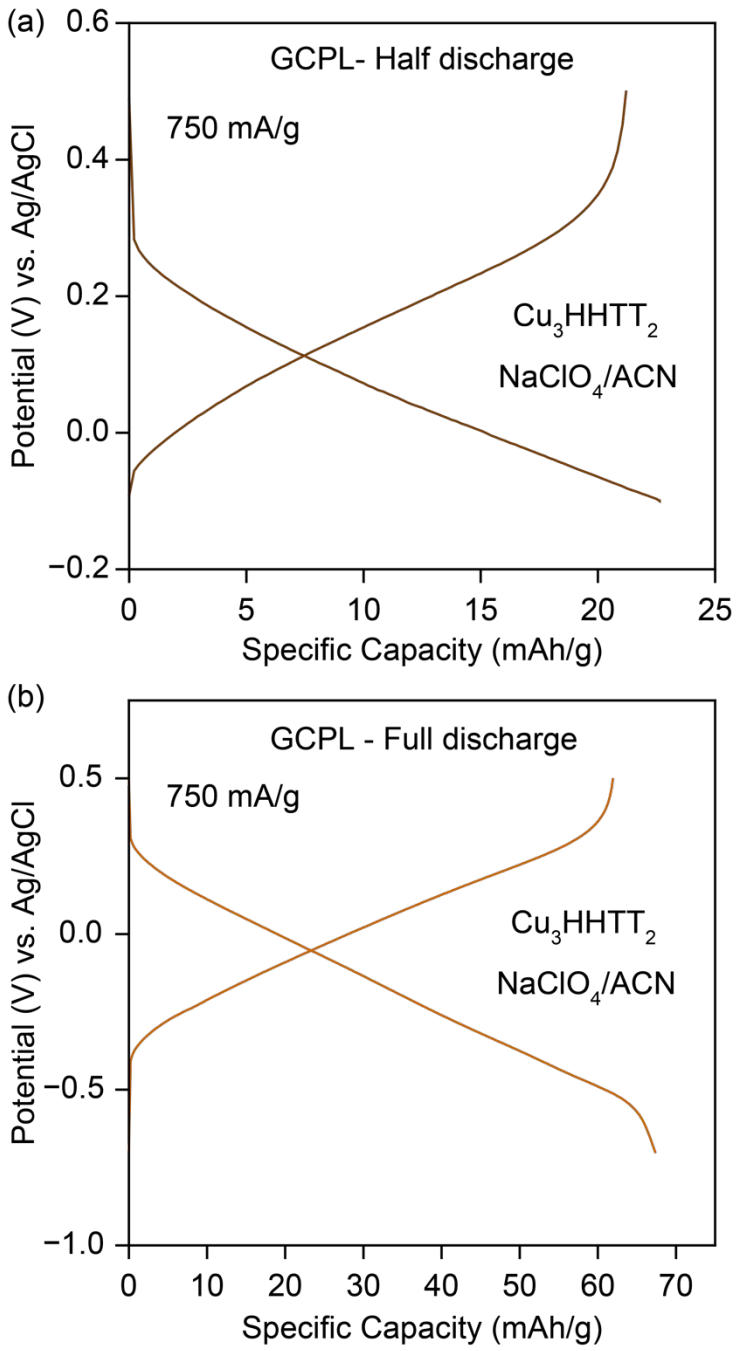

Figure S17. GCPL profile of Cu_3HHTT_2 in $NaClO_4$/ACN at a current density of 750 mA/g in voltage windows of (a) 0.50 to −0.10 V vs. Ag/AgCl (labeled as half discharge) and (b) 0.50 to −0.75 V vs. Ag/AgCl (labeled as full discharge).

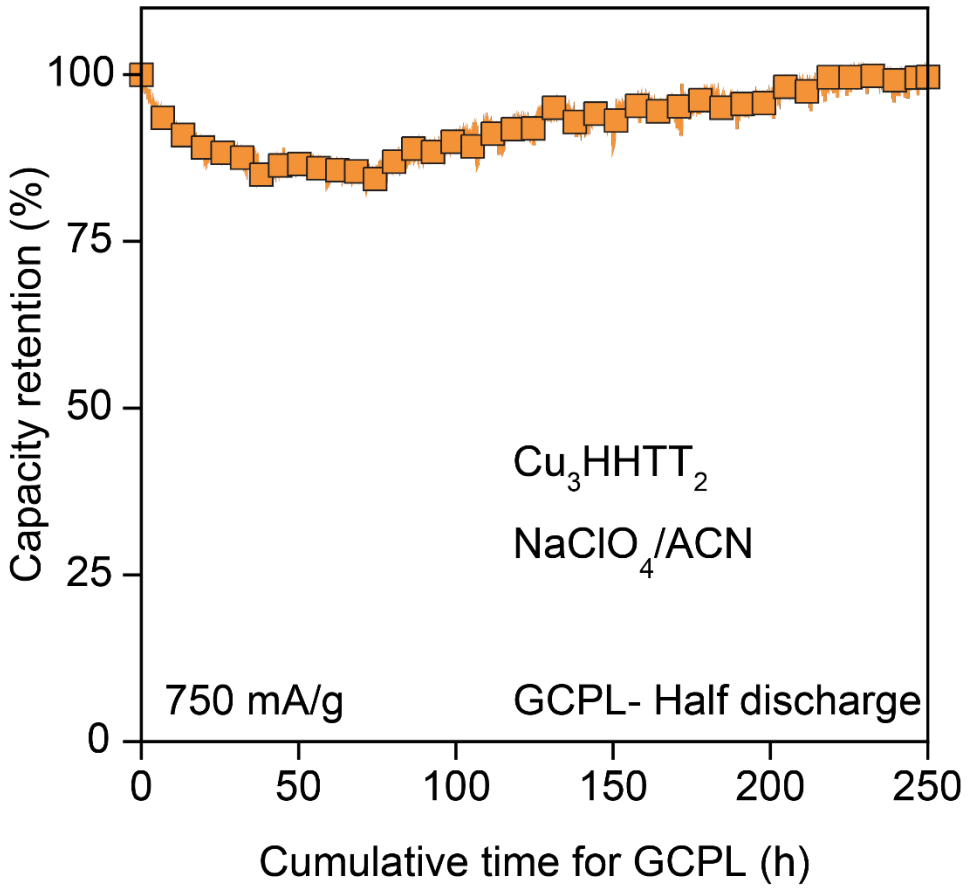

Figure S18. The capacity retention of Cu_3HHTT_2 in $NaClO_4$/ACN at a current density of 750 mA/g in the voltage windows of 0.50 to −0.10 V vs. Ag/AgCl (labeled as half discharge).

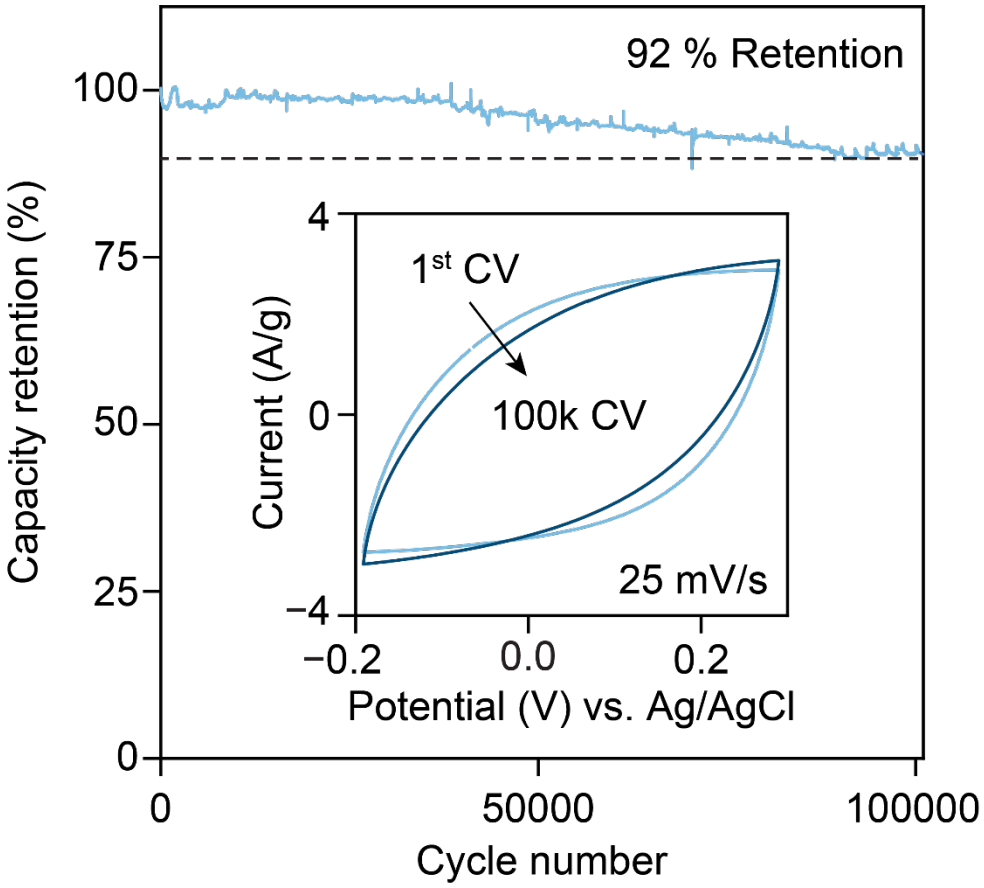

Figure S19. Repeated CV cycling of Cu_3HHTT_2 using $NaClO_4$/ACN in a shorter potential window of 0.3 to −0.2 V vs. Ag/AgCl over 100,000 cycles or 1500 hours.

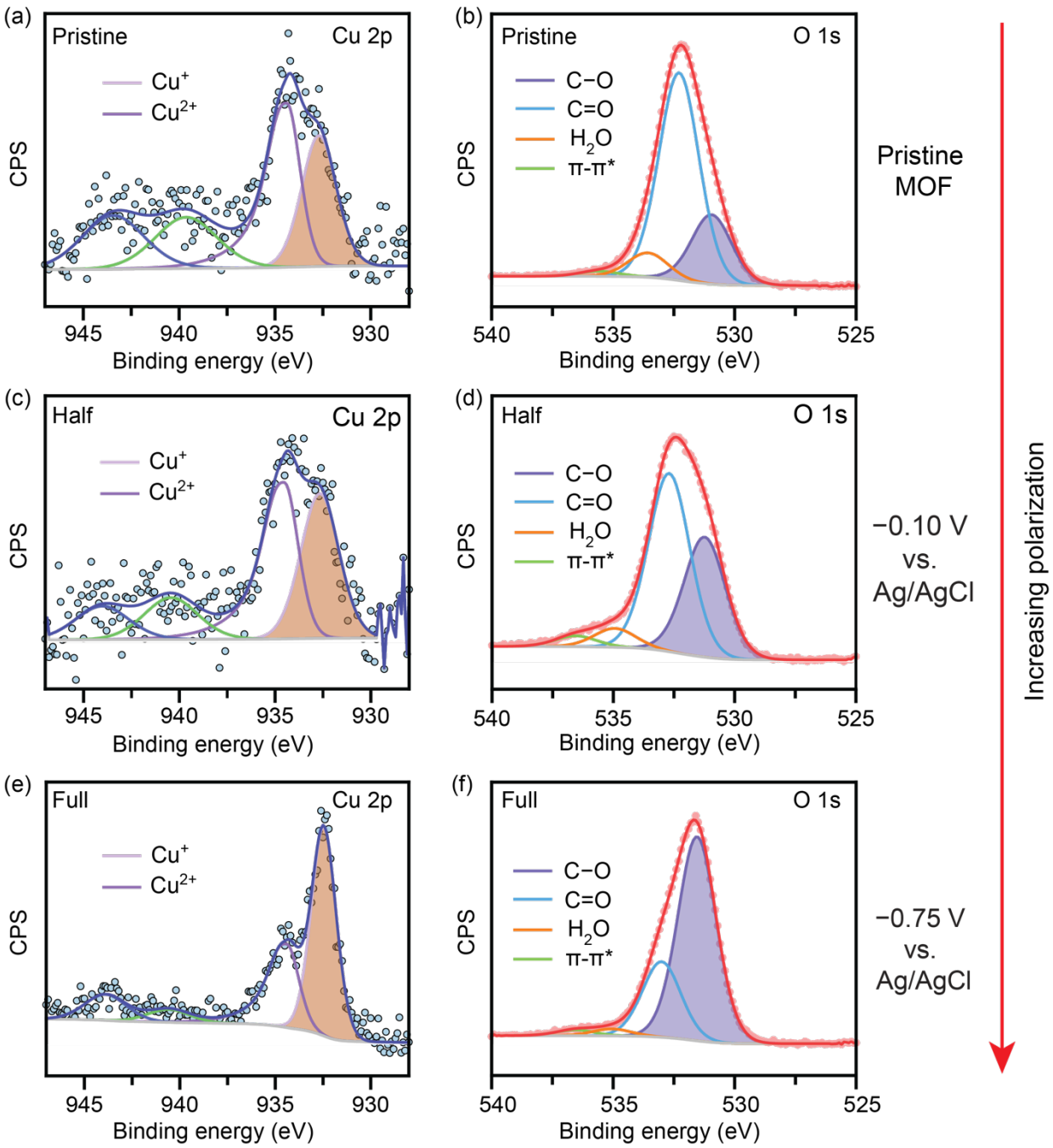

Figure S20. High resolution (HR) (a, c, e) Cu 2p and (b, d, f) O 1s XPS spectra of (a, b) pristine and negatively polarized samples of Cu_3HHTT_2 in $NaClO_4$/ACN till half (c, d) (−0.10 V vs. Ag/AgCl) and (e, f) fully discharged states (−0.75 V vs. Ag/AgCl). A significant reduction of Cu^{2+} to Cu^{+} occurs at potentials below (−0.10 V vs. Ag/AgCl).

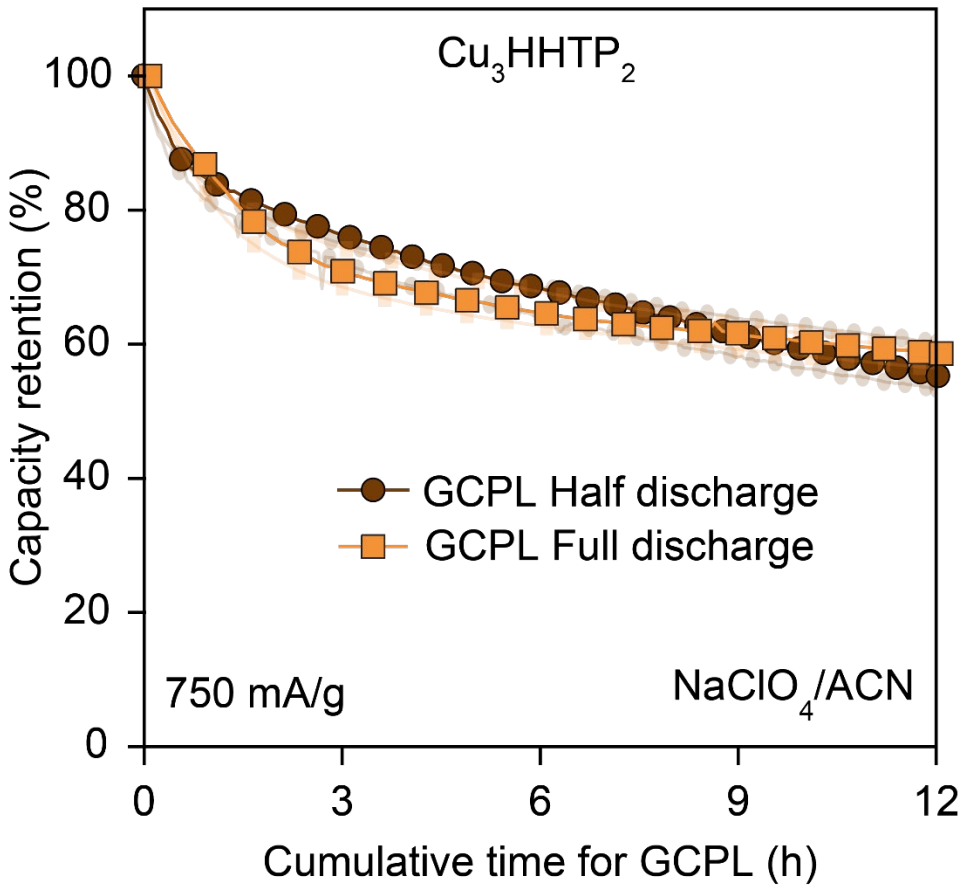

Figure S21. The capacity retention of Cu_3HHTP_2 in $NaClO_4$/ACN from GCPL at a current density of 750 mA/g cycled repeatedly between 0.50 to −0.10 V vs. Ag/AgCl (labeled as half discharge) and (b) 0.50 to −0.70 V vs. Ag/AgCl (labeled as full discharge).

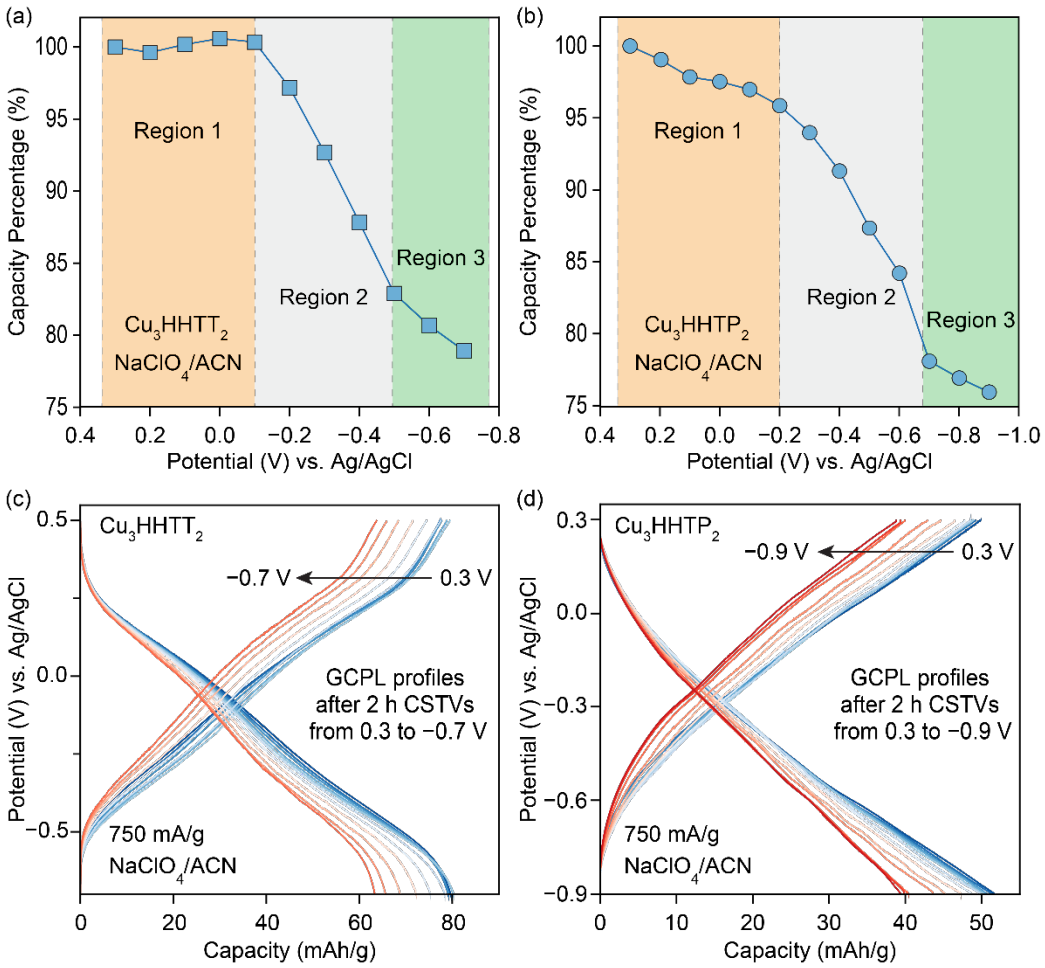

Figure S22. The capacity retention of (a) Cu_3HHTT_2 and (b) Cu_3HHTP_2 from GCPL cycling at a current density of 750mA/g in $NaClO_4$/ACN after application of constant negative potentials (with 100mV interval) for 2 hours. Both MOFs displayed similar capacity retention patterns versus applied potentials, wherein, three distinct regions can be identified. Constant potential polarizations in regions 1 and 3 resulted in minor changes to the capacities, whereas polarizations in region 2 led to a significant drop. The corresponding GCPL profiles for (c) Cu_3HHTT_2 and (d) Cu_3HHTP_2 were recorded between the application of CSTV potentials at a current density of 750 mA/g in $NaClO_4$/ACN.

(a)

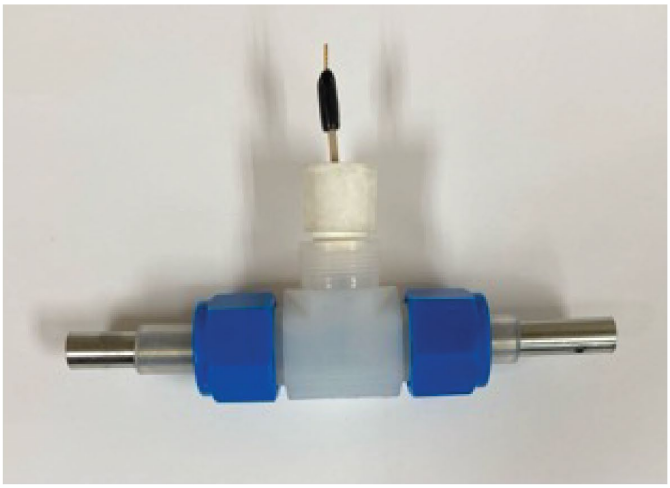

(b)

Figure S23. Digital pictures of the Swagelok cell and the coin cell setups used for electrochemical studies in this work. Swagelok cell enabled tests in three-electrode configuration and typically accommodates ~2 ml of electrolyte. Coin cell setup uses a relatively small amount of electrolyte (50 microliters).

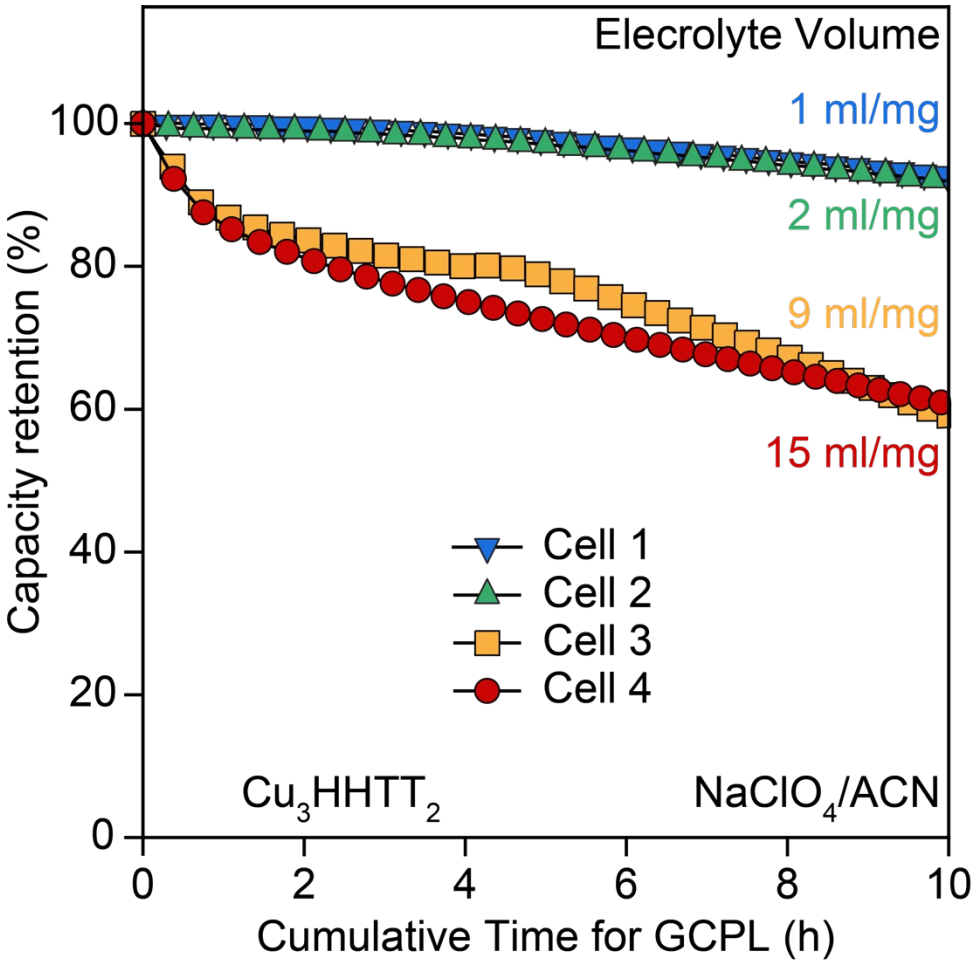

Figure S24. Capacity retention versus cumulative time of GCPL cycling of Cu_3HHTT_2 in $NaClO_4$/ACN is shown for four Swagelok cells. Greater electrolyte volumes correlate to greater capacity losses.

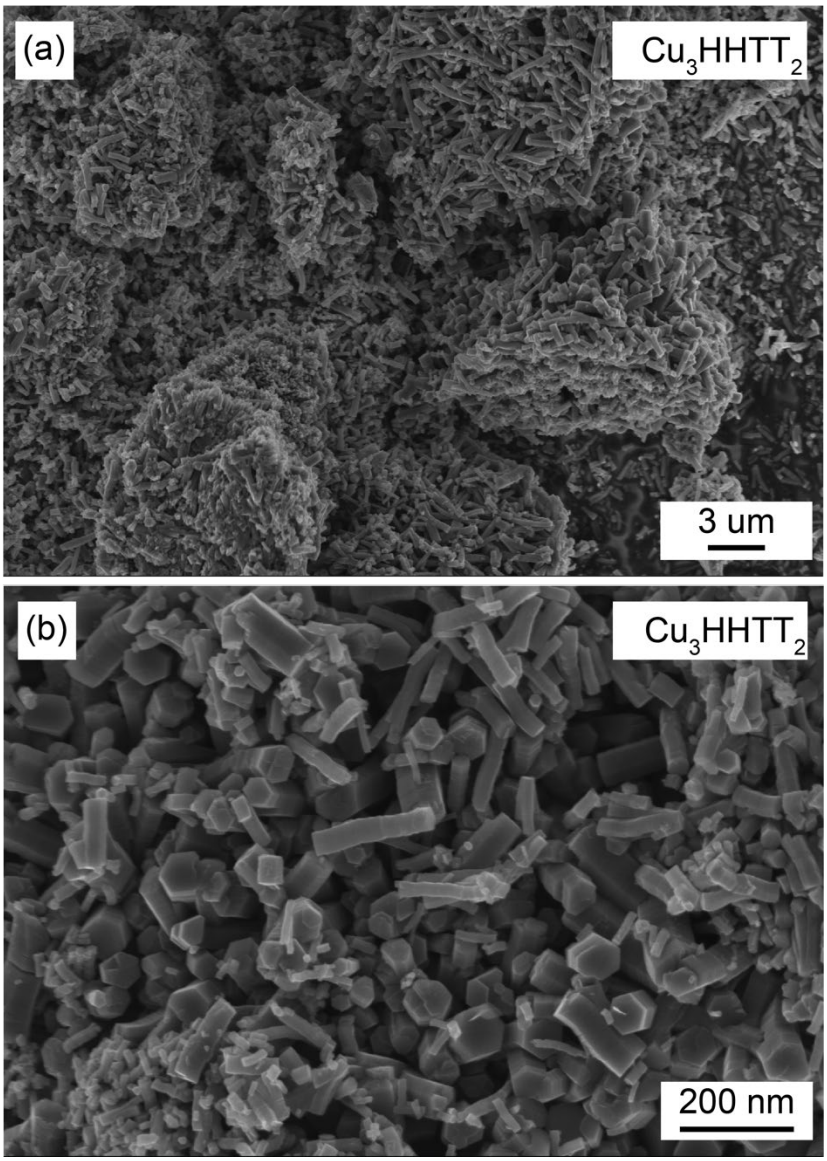

Figure S25. Scanning microscopy images of Cu_3HHTT_2 at two magnifications. The images indicate that the MOF powders used in this study are a mixture of predominantly rods and a few flakes.

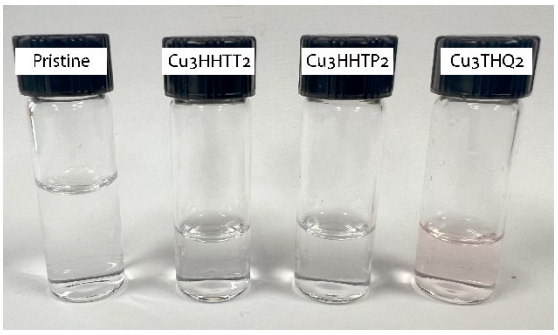

Figure S26. Digital pictures of electrolytes. From left to right is in order of Pristine, Cu_3HHTT_2, Cu_3HHTP_2, and Cu_3THQ_2. A pinkish color is observed for the Cu_3THQ_2 cell.

References

(1) Dou, J.-H.; Arguilla, M. Q.; Luo, Y.; Li, J.; Zhang, W.; Sun, L.; Mancuso, J. L.; Yang, L.; Chen, T.; Parent, L. R.; Skorupskii, G.; Libretto, N. J.; Sun, C.; Yang, M. C.; Dip, P. V.; Brignole, E. J.; Miller, J. T.; Kong, J.; Hendon, C. H.; Sun, J.; Dincă, M. Atomically Precise Single-Crystal Structures of Electrically Conducting 2D Metal–Organic Frameworks. *Nat. Mater.* **2021**, *20* (2), 222–228. https://doi.org/10.1038/s41563-020-00847-7.

(2) Liu, J.; Yang, D.; Zhou, Y.; Zhang, G.; Xing, G.; Liu, Y.; Ma, Y.; Terasaki, O.; Yang, S.; Chen, L. Tricycloquinazoline-Based 2D Conductive Metal–Organic Frameworks as Promising Electrocatalysts for CO2 Reduction. *Angewandte Chemie International Edition* **2021**, *60* (26), 14473–14479. https://doi.org/10.1002/anie.202103398.

(3) Yin, X.; Li, Y.; Cai, W.; Fan, C.; Liu, W.; Wang, N.; Qin, G.; Xie, Z.; Chen, X.; Han, Y. In-Situ Synthesis of Cu-Based Conductive Metal-Organic Frameworks on Graphene Layers for High-Performance Lithium and Potassium Ion Batteries. *Applied Surface Science* **2023**, *624*, 157124. https://doi.org/10.1016/j.apsusc.2023.157124.

(4) Park, J.; Hinckley, A. C.; Huang, Z.; Feng, D.; Yakovenko, A. A.; Lee, M.; Chen, S.; Zou, X.; Bao, Z. Synthetic Routes for a 2D Semiconductive Copper Hexahydroxybenzene Metal–Organic Framework. *J. Am. Chem. Soc.* **2018**, *140* (44), 14533–14537. https://doi.org/10.1021/jacs.8b06666.

(5) Boyd, S.; Ganeshan, K.; Tsai, W.-Y.; Wu, T.; Saeed, S.; Jiang, D.; Balke, N.; van Duin, A. C.; Augustyn, V. Effects of Interlayer Confinement and Hydration on Capacitive Charge Storage in Birnessite. *Nature Materials* **2021**, *20* (12), 1689–1694.